Hadron Physics at GSI

K. Peters[1], *Head of Hadron Physics*
[1]GSI, Darmstadt, Germany; Goethe-University Frankfurt

The hadron physics division is embedded in a strong international network and its main focus is the development, construction and completion of the PANDA experiment at FAIR. In addition, the group is involved in running the BESIII experiment in Beijing, PRChina and the GlueX experiment in Jefferson Lab, Newport News, USA.

PANDA

PANDA is a modern multi-purpose detector for a large variety of hadron physics experiments using an antiproton beam with an incident momentum between 1.5 and 15 GeV/*c*. Hadron physics is a very active field with a lot of important questions on the effective degrees of freedom of QCD at low energies, thus which states exist and what structure they obey. With a luminosity of up to $10^{32}/cm^2/s$ and a momentum spread of $\delta p/p$ being less than 10^{-4} ground-breaking experiments in hadron spectroscopy, hadron structure and hadron dynamics are possible with unprecedented statistics and precision.

PANDA at GSI concentrates, apart from particular detector components, on technical integration, coordination, infrastructure (hostlab activities) and software trigger and core software developments.

GSI is also responsible for R&D and construction of the Barrel DIRC (Detector for internally reflected Cherenkov light). The corresponding TDR was submitted to FAIR in 2016. In addition, groups at GSI are working on APD screening, customized ASIC design (PANDA preamplifier ASIC APFEL, and the PANDA-flash-ADC), the R&D of the GEM detectors and physics analysis and their respective tools. For details please refer to subsequent reports.

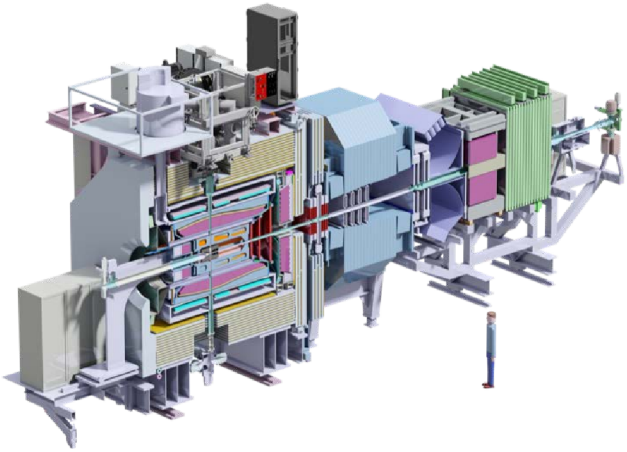

Figure 1: The PANDA detector (cut) for hadron physics experiments at HESR at FAIR.

The GSI group played also a central role in all the various PANDA activities (management, workshops, task forces, reviews) which strengthened the scientific case and underlined the technical competitiveness of the detector layout, which manifested its important role as a first day experiment at FAIR. For those first day experiments a reduced setup including a modified DAQ/Online system with adapted processing power is being proposed to reduce initial detector costs.

BES

The BES3 experiment is investigating all kinds of reactions from e^+e^- annihilations of colliding beams with invariant masses from 3 to 4.6 GeV/c^2. The special interest of GSI is the overlap of the open and hidden charm spectroscopy topics with PANDA and in particular the search for exotic mesons. The previous years were governed by the discovery of various Z_c-States which have a minimum quark-content of at least four quarks, with two of them being a charm-anticharm-pair. GSI is involved in the search for more states and a deeper understanding of the properties and the nature of these states. Particularly η_c yields in Y(4260) decays and the recoil spectra of light mesons or light meson pairs.

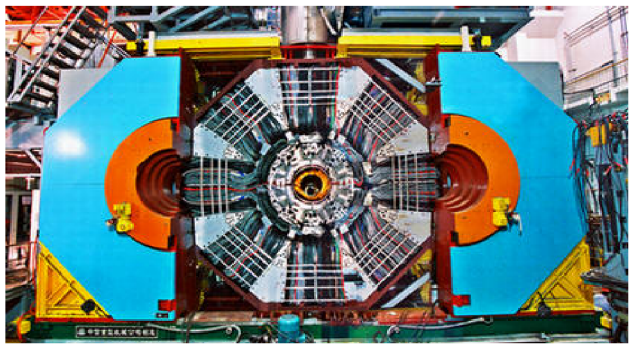

Figure 2: The BES3 detector at IHEP Beijing/China.

GlueX

The GlueX-Experiment in Hall-D at CEBAF at Jefferson National Lab (USA) facilitates a (polarized) photon-beam to produce normal and exotic hadrons of a proton or nuclear target and was successfully commissioned and started physics data taking in 2016.

GlueX will use the coherent bremsstrahlung technique to produce a linearly polarized photon beam. A solenoid-based hermetic detector will be used to collected data on

DOI:10.15120/GR-2017-1

meson production and decays with statistics after the first year of running that will exceed the current photoproduction data in hand by several orders of magnitude. These data will also be used to study the spectrum of conventional mesons, including the poorly understood excited vector mesons and strangeonium. In order to reach the ideal photon energy of 9 GeV for this mapping of the exotic spectrum, 12 GeV electrons are required. Thus, GlueX is part for the JLab12 upgrade being finished recently and is ready for regular operation.

Hybrid mesons, and in particular exotic hybrid mesons, provide the ideal laboratory for testing QCD in the confinement regime since these mesons explicitly manifest the gluonic degrees of freedom. Photoproduction is expected to be particularly effective in producing exotic hybrids. This is due to the fact, that the quantum numbers of the lowest predicted excited modes of the flux tube, when combined with that of a virtual photon, yield exotic JPC. However, there is little data on the photoproduction of light mesons.

The emphasis of the GSI group in GlueX is the development of the GlueX-DIRC together with MIT, JLab, and Indiana University and the search for exotic strangeonium systems and the determination of their static properties, like spin-parity and decays. Significant progress was achieved in 2015 for many systems, which are summarized in the following paragraphs.

The current plan is to place BABAR DIRC bar boxes in front of forward calorimeter to allow for additional PID capabilities. The GlueX PID requirements are rather similar to those of BABAR, thus the concept is comparable but updated in some important technical aspects. Currently the work is focused on prototype optics and software and R&D shall be finalized in 2017.

Figure 3: The GlueX detector at Jefferson Lab.

DOI:10.15120/GR-2017-1

Search for charmonium-like (exotic) states with the BESIII experiment

F. Nerling[1,2], *K. Götzen*[1], *R. Kliemt*[3], *S. Nakhoul*[1,2], *K. Peters*[1,2], *and the BESIII Collaboration*[4]
[1]Goethe Univ. Frankfurt, Germany; [2]GSI, Darmstadt, Germany; [3]HIM, Mainz, Germany; [4]IHEP, Beijing, China

The BESIII experiment [1] at BEPCII at IHEP in Beijing/China has collected the world largest data sets in the τ-charm region, and it is well suited to cover a rich hadron physics programme, including charmonium and open-charm spectroscopy, R-scan and electromagnetic form factor measurements. Especially in the "XYZ" region above 3.8 GeV, BESIII has accumulated unique data sets to explore the still-unexplained XYZ states.

For understanding the nature of some of these states, a precise measurement of the line-shapes is needed as it is only possible in a direct formation experiment. Moreover, complete multiplets also of higher spin states are mandatory. As discussed earlier [2], the $p\bar{p}$ annihilation experiment PANDA/FAIR will provide unique and complementary measurements in view of both, see e.g. [3], as a matter of principle not possible with an e^+e^- annihilation experiment like BESIII.

Apart from the first charged charmonium-like state $Z_c(3900)$ discovered at BESIII in the reaction $e^+e^- \to J/\psi\pi^+\pi^-$ at $\sqrt{s} = 4.26$ GeV, corresponding to the the $Y(4260)$ resonance, also a second has been observed, the $Z_c(4020)^\pm$ decaying to $h_c\pi^\pm$. Together with the neutral isospin partners decaying to $J/\psi\pi^0$ and $h_c\pi^0$, respectively, two isospin triplets have been established [4]. Further decay channels are under investigation. At GSI, we are exploring possible decay channels of the Z_c states involving η_c together with various recoil particles — first results are in preparation for internal review and planned to be published soon.

The $Y(4260)$ and the $Y(4360)$ had firstly been observed using initial state radiation (ISR) decaying to $J/\psi\pi^+\pi^-$ and $\psi(2S)\pi^+\pi^-$, respectively, by BABAR [5]. Based on the "high luminosity" (8.2 fb^{-1}) and the "low luminosity" (0.8 fb^{-1}) XYZ data, we performed a precision measurement of the energy dependent cross-section $\sigma(e^+e^- \to J/\psi\pi^+\pi^-)$ in the energy range of $3.77 < E_{\rm cms} < 4.60$ GeV recently published [6]. The result obtained by a simultaneous fit to both data sets is shown in Fig. 1. The signal yields are determined using an unbinned maximum-likelihood fit ("high luminosity" XYZ data) and a simple counting method ("low luminosity" scan data), for the latter the background counts from sidebands are subtracted. The cross-section appears inconsistent with a single peak just for the $Y(4260)$ — two resonances to describe two peaks is favoured over one by the data at high statistical significance of more than 7 σ. Given the much larger statistics by BESIII, the $Y(4260)$ and the $Y(4360)$ are resolved here for the first time, and the $Y(4360)$ is first observed decaying to $J/\psi\pi^+\pi^-$. At GSI, we contribute to the clarification of this important cross-section via the inclusive measurement of $Y(4260) \to J/\psi\pi^+\pi^-, h_c\pi^+\pi^-$ and further recoil systems. First promising results will be presented internally to the collaboration still this year.

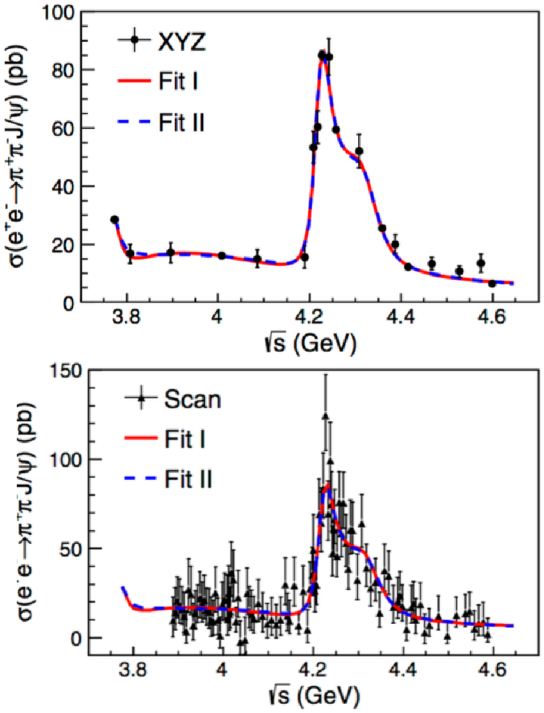

Figure 1: Precision cross-section measurement of the $J/\psi\pi^+\pi^-$ production in e^+e^- annihilation as obtained from a simultaneous fit to both: "high luminosity" (top) XYZ data and "low luminosity" (down) scan data (reprinted with kind permission of APS from [6], copyright 2017 American Physical Society).

Before PANDA starts, there is the great chance to complete the observation of entire (low spin) multiplets and to explore further decay channels of XYZ states with BESIII, offering a perfect preparation of physics analysis of PANDA data, and thus keeping and gaining important experience on this newly very active field of research.

References

[1] BESIII Collab., M. Ablikim *et al.*, NIM **A614** (2010) 345.
[2] F. Nerling *et al.*, GSI Scientific Report 2015-1, (2015) 117.
[3] F. Nerling *et al.*, *A precision line-shape measurement of the $X(3872)$ with PANDA/FAIR*, this Scientific Report (2017).
[4] BESIII Collab., M. Ablikim *et al.*, PRL **110** (2013) 252001, and PRL **111** (2013) 242002; PRL **115** (2015) 112003, and PRL **113** (2014) 212002.
[5] BABAR Collab., B. Aubert *et al.*, PRL 95 (2005) 142001, and PRL 98 (2007) 212001.
[6] BESIII Collab., M. Ablikin *et al.*, PRL 118 (2017) 092001.

DOI:10.15120/GR-2017-1

Search for exotic mesons with the GlueX/JLab experiment

F. Nerling[1,2], *K. Götzen*[2], *A. Hamdi*[1,2], *K. Peters*[1,2], *and the GlueX Collaboration*[3]
[1]Goethe Univ. Frankfurt, Germany; [2]GSI, Darmstadt, Germany; [3]Jefferson Lab, Newport News, USA

The GlueX experiment is located at the Jefferson National Accelerator Facility (JLab). The primary focus is to understand the nature of confinement in QCD by mapping the spectrum of exotic mesons generated by the excitation of the gluonic field binding the quarks. Using photoproduction to produce exotic states, the experiment probes new areas. The GlueX detector was installed in the new Hall-D at JLab as part of the 12 GeV energy accelerator upgrade. After the first commissioning run in 2014, and first received 12 GeV electrons in 2015, GlueX has begun first physics data taking in 2016.

As compared to $\bar{p}p$ and e^+e^- annihilation, cf. [1], and also pion beam experiments like COMPASS, photoproduction represents another complementary probe and production mechanism for (exotic) hadrons. Given the overlap in accessible invariant masses in GlueX (up to $\sim$2.5 GeV/c^2) and PANDA (up to $\sim$5.5 GeV/c^2, also BESIII up to $\sim$4.6 GeV/c^2), the charmonium, strange and light spectroscopy studies planned with PANDA are complementarily completed with the strange/light quark sector the GlueX experiment is designed for.

At GSI, we are especially interested in searches for tetraquark and hybrid candidates decaying to $K\bar{K}\pi(\pi)$ final states, for which a good K/π identification is needed that later will be improved by the major detector upgrade of an additional DIRC detector we are majorly involved in, see also [2]. Apart from planned physics analysis, a present service work task is to improve the dE/dx measurements for particle identification — first promising results have been obtained and appreciated by the collaboration.

Based on the spring 2016 data, a measurements of the photon beam asymmetry Σ for the reactions $\vec{\gamma}p \to p\pi^0$ and $\vec{\gamma}p \to p\eta$ using a 9 GeV linearly-polarised, tagged photon beam incident on a liquid hydrogen target in Hall-D has been performed, recently accepted for publication [3], and representing not only the first measurement by GlueX but also the first one with a 12 GeV electron beam at JLab[1].

The resultant asymmetries (Fig. 1) as a function of the proton momentum transfer have been measured at higher precision than previous π measurements and are the first η measurements in this energy regime [3]. The black filled circles are the measured asymmetries, the black error bars represent the combined statistical and systematic uncertainties, and the grey bars indicate the uncorrelated systematic errors. Also shown are the previous SLAC results at 10 GeV (blue open circles) along with various Regge theory calculations. The results are compared with theoretical predictions based on t-channel, quasi-particle exchange

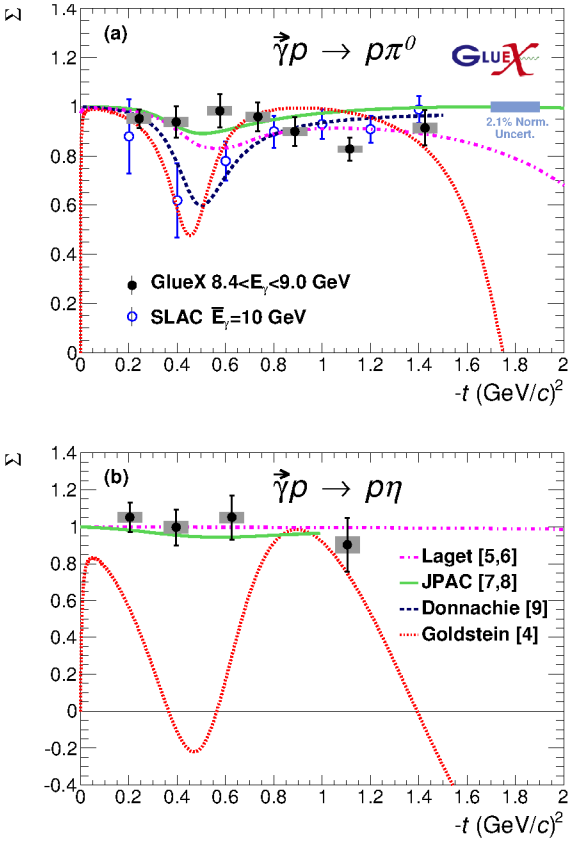

Figure 1: Beam asymmetry Σ for (a) $\vec{\gamma}p \to \pi^0$ and (b) $\vec{\gamma}p \to p\eta$ (reprinted with kind permission of APS from [3], copyright 2017 American Physical Society).

and constrain the axial-vector component of the neutral meson production mechanism in these models.

Before PANDA starts, there is the great chance to already explore the strangeonium spectrum and search for exotic hybrid states using photoproduction, offering a perfect preparation of physics analysis of PANDA data, including reconstruction software for e.g. particle identification, and thus keeping and gaining important experience.

[1] 12 GeV electrons are required to reach the photon energy of 9 GeV.

References

[1] F. Nerling, *et al.*, *A precision lineshape measurement of the $X(3872)$ with PANDA/FAIR*; and F. Nerling, *et al.*, *Search for charmonium-like (exotic) states with the BESIII experiment*, this Scientific Report (2017).

[2] R. Dzhygadlo, *et al.*, *The DIRC Upgrade for the GlueX Experiment*, DPG Münster (2017).

[3] GlueX Collab., H. Al Ghoul, *et al.*, Phys. Rev. C95 (2017) 042207, DOI:https://doi.org/10.1103/PhysRevC.95.042201.

DOI:10.15120/GR-2017-1

DIRC-based PID for the EIC Central Detector*

R. Dzhygadlo†[1], *K. Peters*[1,2], *C. Schwarz*[1], *and J. Schwiening*[1]
[1]GSI, Darmstadt, Germany; [2]Goethe-Universität, Frankfurt, Germany

The Detector of Internally Reflected Cherenkov light (DIRC) is expected to be a key element of the PID system for the future Electron-Ion Collider (EIC) central detector [1]. The EIC PID consortium (eRD14 [2]) investigates the feasibility of a high-performance DIRC that would extend the momentum coverage well beyond state-of-the-art, providing 3 standard deviations separation of π/K up to 6 GeV/c, e/K up to 1.8 GeV/c and p/K up to 10 GeV/c.

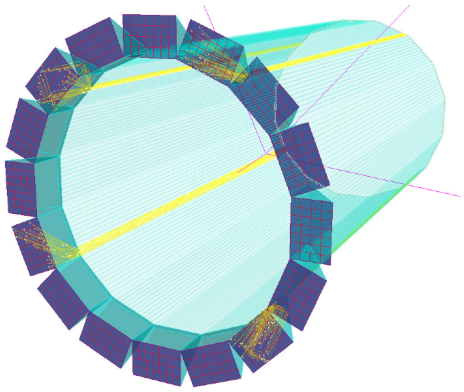

Figure 1: Geant-based simulation of the EIC DIRC using narrow bars as radiators together with prisms as expansion volumes. Cherenkov photon trajectories from 4 GeV/c kaons are shown in yellow.

Geant4 simulations are used to optimize the design configuration of the DIRC counter in terms of the performance and the best integration with the EIC detector. Fig. 1 shows the Geant4 implementation of the baseline design of a DIRC with narrow bars, sherical focusing lenses, and compact fused silica prisms. Possible improvements on the current DIRC design include multi-anode sensors with smaller pixels, providing fast single-photon timing in high magnetic fields, and chromatic dispersion mitigation.

Two different reconstruction approaches have been developed to evaluate the detector resolution for various design optimizations [3]. An example of such an optimization is shown in Fig. 2, where the impact of the pixel size on the Cherenkov angle resolution per photon (SPR) is shown for several polar angles.

To evaluate the PID performance of the design the track Cherenkov angle resolution σ_{θ_C} is defined as $\sigma^2_{\theta_C} = \mathrm{SPR}^2/N_\gamma + \sigma^2_{track}$, where N_γ is the number of detected photons per track and σ_{track} is the uncertainty of the track direction in the DIRC, dominated by multiple scattering and the resolution of the tracking detectors.

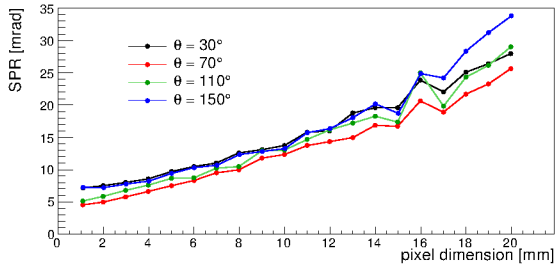

Figure 2: Single photon Cherenkov angle resolution as a function of the pixel dimension. Colors indicate different polar angles of the charged particle.

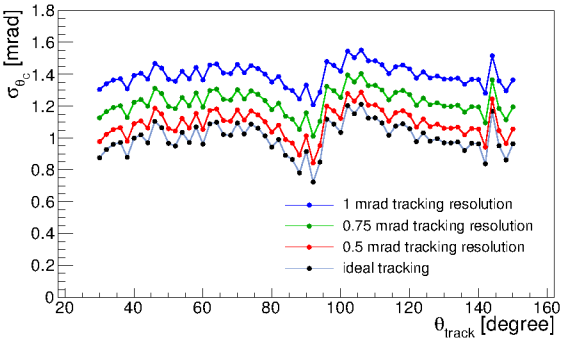

Figure 3: Cherenkov angle resolution per particle for different tracking resolutions.

The optimized design, featuring pixels of 3 mm size, narrow radiators, and 3-layer spherical lenses, is expected to achieve a Cherenkov angle resolution per particle of 1.2 mrad or better for all polar angles, assuming a tracking resolution of 0.5 mrad (see Fig. 3). This corresponds to at least 3 s.d. π/K separation up to 6 GeV/c momentum for forward-going particles, which satisfies the DIRC@EIC performance goal.

References

[1] A. Adare et al., arXiv:1402.1209 [nucl-ex]
[2] G. Kalicy et al., 2016 JINST 11 C07015
[3] R. Dzhygadlo et al., Nucl. Instr. and Meth. Phys. Res A 766 (2014) 263

* Work supported by HGS-HIRe, HIC for FAIR, and by BNL under eRD4 and eRD14.
† R.Dzhygadlo@gsi.de

Performance of the PANDA Barrel DIRC Prototype*

C. Schwarz[†1], *J. Schwiening*[‡1], *A. Ali*[1,2], *A. Belias*[1], *R. Dzhygadlo*[1], *A. Gerhardt*[1], *M. Krebs*[1,2], *D. Lehmann*[1], *K. Peters*[1,2], *G. Schepers*[1], *and M. Traxler*[1]

[1]GSI, Darmstadt, Germany; [2]Goethe Universität Frankfurt, Germany

Charged Particle Identification (PID) for the barrel section of the PANDA target spectrometer [1, 2] will be provided by a DIRC (Detection of Internally Reflected Cherenkov light) detector. This counter will cover the angular range of 22–140° and cleanly separate charged pions from kaons for momenta up to 3.5 GeV/c with a separation power of at least 3 standard deviations (s.d.).

The design of the PANDA Barrel DIRC detector is based on the successful BABAR DIRC [3] and the R&D for the SuperB FDIRC with several important improvements to optimize the performance for PANDA, such as a focusing lens system, fast timing, and a compact synthetic fused silica prism as expansion region.

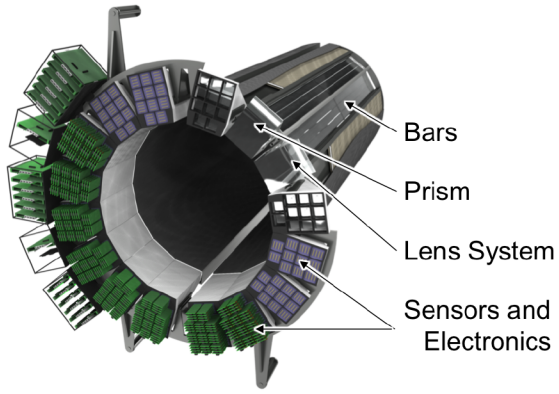

Figure 1: The PANDA Barrel DIRC baseline design in the Geant4 simulation.

In the PANDA Barrel DIRC baseline design, shown in Fig. 1, the barrel of 47.6 cm radius comprises 16 flat sections with 3 fused synthetic silica radiator bars ($17 \times 53 \times 2400$ mm^3) each. A flat mirror is attached to the forward end of each bar to reflect photons towards the readout end, where they are focused by a multi-component spherical lens onto the back of a 30 cm-deep solid synthetic fused silica prism, serving as expansion volume. An array of lifetime-enhanced Microchannel Plate Photomultiplier Tubes (MCP-PMTs) is used to detect the photons and measure their arrival time with a precision of about 100 ps in the magnetic field of about 1 T.

Due to the tight optical and mechanical tolerances, the cost of radiator fabrication is, together with the cost of the photon detectors, the dominant contribution to the Barrel DIRC construction cost. Replacing the 3 radiator bars per section by one 16 cm-wide plate would significantly reduce the radiator fabrication cost since fewer pieces have to be produced. However, the optical quality of such plates and the PID performance of a design with wide plates need to be validated before this option can be considered for PANDA.

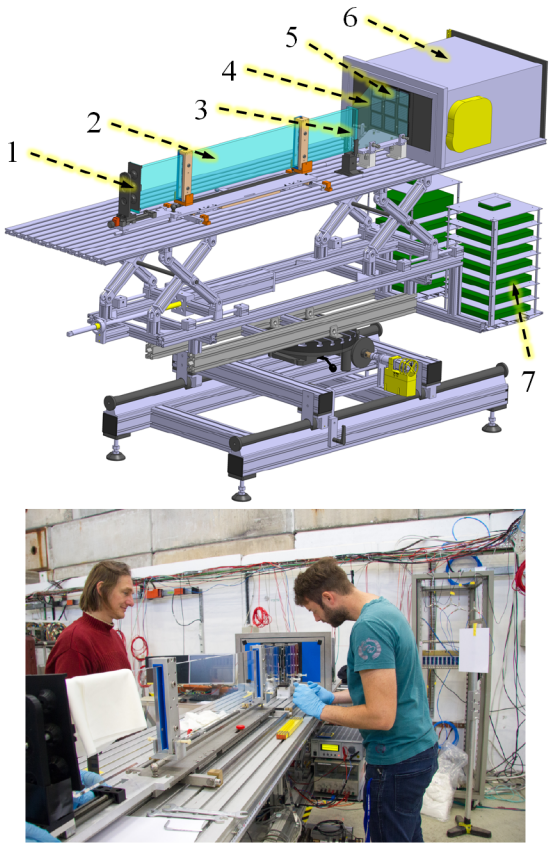

Figure 2: *T*op: Schematic of the prototype used at CERN in 2016, with 1: flat mirror, 2: radiator plate, 3: lens, 4: expansion volume, 5: array of 3×3 MCP-PMTs, 6: readout unit, and 7: TRB stack. *B*ottom: Photograph of the prototype in the T9 beamline.

In the fall of 2016 the latest Barrel DIRC prototype, shown in Fig. 2, was evaluated in a mixed hadron beam at the CERN PS. The setup comprised a synthetic fused silica plate ($17 \times 175 \times 1225$ mm^3) as radiator with an optional 2-layer cylindrical lens attached to one end and a flat mirror to the other end as well as a large synthetic fused silica prism as expansion volume. The plate, lens, and prism were coupled to each other using optical grease and placed into a light-tight container on a remote-controlled rotating stage.

* Work supported by HGS-HIRe, HIC for FAIR, and BNL grant eRD14.

† C.Schwarz@gsi.de

‡ J.Schwiening@gsi.de

DOI:10.15120/GR-2017-1

The location and arrival time of photons were measured with a precision of about 2 mm and 180 ps, respectively, using an array of 9 PHOTONIS XP85012 MCP-PMTs, coupled with optical grease to the back surface of the prism. The data acquisition was performed using PADIWA frontend cards and TRB3 boards [4].

During 18 days of data taking a total of some 4.9×10^8 triggers were recorded in the mixed hadron beam at the T9 area of the CERN PS. Most of the time the beam was set to a π/p momentum of 7 GeV/c and to beam/plate polar angles below 40° to evaluate the π/K separation performance[1] of the wide plate for the high momentum range of final state particles in the forward direction of PANDA, the most challenging phase space region for the Barrel DIRC.

The time-based imaging method was used to determine the PID performance of the wide plate, in particular the π/p separation power. This method is based on the approach used by the Belle II Time-Of-Propagation (TOP) counter [5] and compares the measured arrival time of Cherenkov photons in each single event to the expected photon arrival time for every pixel and for every particle hypothesis, yielding the PID likelihoods. Using a time-of-flight system to cleanly tag the pions and protons in the beam, the log-likelihood difference for the pion and proton hypotheses were calculated for the two tagged samples.

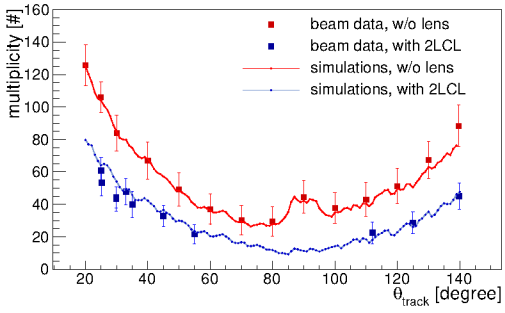

Figure 3: Photon yield as a function of the track polar angle for the wide plate without lens (red) and with the 2-layer cylindrical lens ("2LCL", blue) for tagged protons at 7 GeV/c beam momentum in data (points) and Geant4 prototype simulation (lines).

The reconstructed photon yield as a function of the track polar angle is shown in Fig. 3 for the configuration with the wide radiator plate, with and without the 2-layer cylindrical lens. The simulation describes the experimental data well, with remaining differences of up to 10%. The photon yield for the 2-layer cylindrical lens is, as expected, substantially lower than the yield for the plate coupled directly to the prism. While most of this difference is due to the loss of photons inside the lens, a significant fraction of the photons are lost at the interface of the lens and the prism due to a size mismatch between the prototype lens and the synthetic fused silica prism.

[1] The π/p Cherenkov angle difference at 7 GeV/c (8.1 mrad) is close to the π/K Cherenkov angle difference at 3.5 GeV/c (8.5 mrad).

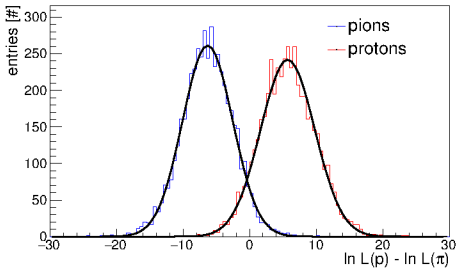

Figure 4: Proton-pion log-likelihood difference distributions for proton-tagged (red) and pion-tagged (blue) beam events from 2016 as a result of the time-based imaging method. The distributions are for the wide plate with the 2-layer cylindrical lens, a beam with 7 GeV/c momentum and 25° polar angle. The separation power value from the Gaussian fits is 3.1 ± 0.1 s.d..

The result of the unbinned likelihood calculation for the plate with the 2-layer cylindrical lens at 7 GeV/c momentum and 25° polar angle is shown in Fig. 4. The observed π/p separation power is $3.1^{+0.1}_{-0.1}$ s.d., in good agreement with the Geant4 simulation of the prototype, which predicts a $3.3^{+0.1}_{-0.1}$ s.d. separation value.

The result of the 2016 beam test validates the plate with a cylindrical focusing lens as a potential design for the PANDA Barrel DIRC. However, the PID performance of the previous prototype, which used a narrow bar and a 3-layer spherical lens, was significantly better during a beam test at CERN in 2015 [6]. Furthermore, the design with narrow bars provides a larger margin for error and can be expected to have a significant performance advantage during the initial phase of the PANDA experiment due to the dependence of the wide plate geometry on excellent timing precision. Therefore, the geometry with narrow bars and 3-layer spherical lenses was selected as the baseline design for the PANDA Barrel DIRC.

References

[1] PANDA Collaboration, *Technical Progress Report, FAIR-ESAC/Pbar*, (2005).

[2] PANDA Collaboration, *Physics Performance Report for PANDA: Strong Interaction Studies with Antiprotons*, arxiv:0903.3905.

[3] I. Adam et al., *Nucl. Instr. and Meth. Res. Sect. A* **538** (2005) 281.

[4] M. Cardinali et al., *Nucl. Instr. and Meth. Res. Sect. A* **766** (2014) 231

[5] M. Staric et al., *Nucl. Instr. and Meth. Res. Sect. A* **639** (2011) 252

[6] J. Schwiening et al., "The PANDA Barrel DIRC," 9th International Workshop on Ring Imaging Cherenkov Detectors (RICH 2016).

Measurement results of the optical quality of prototype radiators for the PANDA Barrel DIRC detector*

M. Krebs[†1,2], *K. Peters*[1,2], *G. Schepers*[‡1], *C. Schwarz*[1], *and J. Schwiening*[1]
[1]GSI, Darmstadt, Germany; [2]Goethe-Universität, Frankfurt, Germany

In the barrel region of the target spectrometer of the PANDA experiment, a fast focusing Cherenkov counter using the DIRC (Detection of Internally Reflected Cherenkov light) principle will provide charged hadronic particle identification (PID). In order to meet the PANDA PID requirements, the Barrel DIRC has to provide precise measurements of the Cherenkov angle, which is the crucial quantity for identifying charged particles that traversed the radiators. The Cherenkov photons propagate through the radiators by total internal reflection until they reach the detection plane, which is equipped with an array of photon sensors.

The Cherenkov angle resolution and the photon yield are critical figures of merit for the PID performance of the DIRC. Thus the radiators, rectangular bars made from synthetic fused silica, have to fulfill very strict optical and geometrical requirements as Cherenkov photons can undergo up to several hundred reflections before they reach the readout end. To ensure high transport efficiency and maintain the magnitude of the Cherenkov angle during all reflections, properties such as highly polished surfaces, parallelism of the sides, and sharp corners have to meet the requirements.

The optical quality of the radiators is assured with two setups, measuring the roughness of surfaces (Fig. 1) as well as the rectangularity and parallelism (Fig. 3). In order to determine the surface roughness of one radiator, it is necessary to measure firstly the bulk transmission and secondly the transmitted intensity after many internal reflections. Hence, an optical setup using lasers of four different wavelengths and a computer-controlled motion system is operated in the optics lab. For the bulk transmission measurement, the laser beam is coupled straight into the radiator measuring the attenuation of the intensity in the bulk material. This intensity loss is related to the attenuation length reaching several hundred meters for synthetic fused silica in the visible wavelength range.

Depending on the length and orientation of the radiator, the beam is reflected from the faces (wide sides) up to 50 times, until it leaves the bar and hits the (value) photo diode. A reference diode is used to correct for fluctuations from the laser system. The fraction of light lost during all internal reflections is translated into a reduction of the coefficient of total internal reflection, which in turn can be related to the surface roughness via the scalar scattering theory. An extensive prototype radiator program had been started resulting in about a total of 30 prototype radiators from various manufacturers. These manufacturers use different materials and techniques for radiator production, hence quality assurance measurements at GSI are needed to qualify vendors for the production stage. Figure 2 shows results for the reflection coefficients from different prototype bars and plates built by five manufacturers such as Carl Zeiss Jena GmbH, InSync Inc., Nikon Corp., Zygo Corp., and Aperture Optical Sciences/Okamoto. For instance, showing a surface roughness of 3 Å, InSync # 2 (InSync Inc.) exceeds the PANDA Barrel DIRC radiator specifications of 10 Å for the large sides of the radiator. Nikon Corp. and InSync Inc., who have built the prototype plates, also fulfill the PANDA Barrel DIRC specifications for the roughness of the surfaces. The measured reflection coefficients (points) and expectations from scalar scattering theory (lines) can be seen in Fig. 2. The surface roughness values are found to be in good agreement with the quality assurance data from the vendors. As vendors measure the surface roughness using an interferometric approach, they can only determine the outer roughness of the radiator surfaces, while the inner surface roughness is more important for DIRC applications as photons propagate via total internal reflection. Expanding the Barrel DIRC optical setup by adding a 266 nm (ultra-violet) laser, lead to an increase in sensitivity of measuring possible sub-surface damage inside the material. Yet the 266 nm laser was only available for the plate measurements. The cause for the deviation of the 266 nm data points from the prediction of the scalar scattering theory is under investigation.

The parallelism and squareness of the radiator sides and faces have to fulfill strict requirements, too. Simulation studies showed that the deviation of the side-to-face angles $\Delta\Phi$ from the nominal 90° value must not exceed 0.25 mrad and the non-parallelism $\Delta\Theta$ required to be smaller than 0.5 mrad to keep the angular smearing due to the large number of reflections as small as possible. For the quality assurance of the rectangularity and parallelism of the radiator surfaces, a Nikon 6D autocollimator (see Figs. 3 and 4) is used. This optical instrument has the capability to measure small angular displacements with an accuracy of 0.002 mrad without making contact with the very sensitive surfaces of the radiators. Fig. 3 shows a sketch of the autocollimator setup and the principle of the measurement. In combination with a pentaprism, the deviation of the angle between a face and a side of the radiator

* Work supported by HGS-HIRe
† m.krebs@gsi.de
‡ g.schepers@gsi.de

DOI:10.15120/GR-2017-1

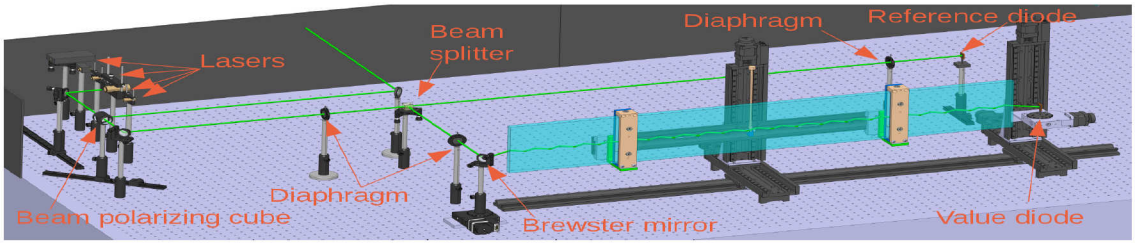

Figure 1: Catia drawing of the setup used for the surface roughness measurement of the Barrel DIRC radiators. The setup accommodates the wide plate radiator in this example.

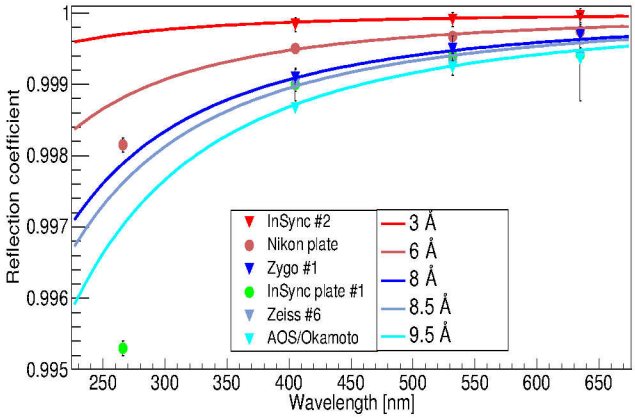

Figure 2: Reflection coefficients for several prototype radiators including 2 wide plates. The lines represent the expected reflection coefficients for defined surface roughness values from the scalar scattering theory.

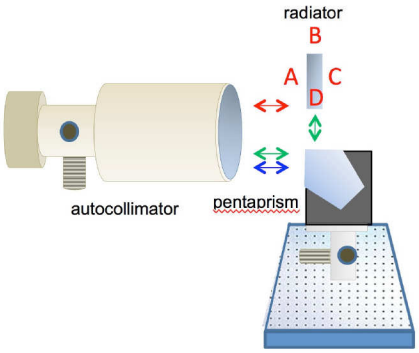

Figure 3: Measurement principle for obtaining the squareness and parallelism of the prototype radiators.

from 90° can be measured precisely. The parallelism of two sides (faces or ends) behind eachother can be read directly. Since each property is read off as a deviation of two simultaneous measured lines additional systematic errors are excluded. The setup allows to place the bars and autocollimator independently from each other and thus enables the detection of variations of the squareness and parallelism (thickness variation). So far, two bars were studied in detail, including measurements at several points along the length of the bars, and the results are shown in Tab. 1. The first prototype bar measured in this setup was produced by Zeiss and all angles were found to deviate from the nominal 90° value by less than 0.024 mrad in agreement with the manufacturers data, thus meeting the production specifications and proving the quality assurance data of the company. While the Zeiss bar is found to have excellent values of non-squareness and parallelism, easily meeting the PANDA Barrel DIRC requirements, the LZOS bar fails the $\Delta\Phi$ production tolerances by a factor of 2-4. The remaining prototype bars/plates will be similarly evaluated in the two setups in the future.

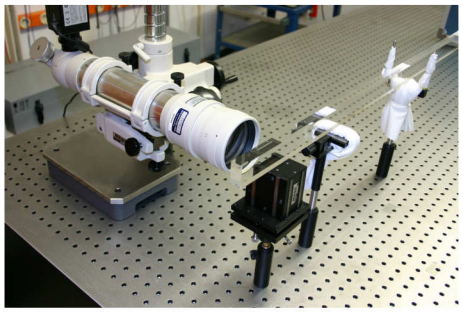

Figure 4: Photograph of the autocollimator setup in the lab.

Angle between sides	Zeiss $\Delta\Phi$ [mrad]	LZOS $\Delta\Phi$ [mrad]
A/B	0.073 ± 0.005	-1.098 ± 0.005
B/C	0.036 ± 0.005	1.037 ± 0.005
C/D	0.007 ± 0.005	-0.541 ± 0.005
D/A	0.075 ± 0.005	0.582 ± 0.005
	$\Delta\Theta$ [mrad]	$\Delta\Theta$ [mrad]
A/C	0.023 ± 0.005	0.041 ± 0.005
B/D	0.030 ± 0.005	0.492 ± 0.005

Table 1: Results from the autocollimator measurements for prototype bars from LZOS and Zeiss

References

[1] M. Krebs, "Quality Assurance Measurements for the PANDA Barrel DIRC Quartz Radiators", HK27.55, DPG Spring Meeting, Muenster, Germany, March 2017

[2] J. Schwiening for the PANDA Cherenkov group, "The PANDA Barrel DIRC Detector", RICH2016, Bled, Slovenija, September 2016

[3] R. Hohler, "Prototyp-Radiatoren eines Barrel-DIRC für das PANDA-Experiment", PhD thesis, Frankfurt, Germany, 2011

DOI:10.15120/GR-2017-1

Latest results with microchannel plate PMTs*

A. Lehmann†[1], *M. Böhm*[1], *W. Eyrich*[1], *D. Miehling*[1], *M. Pfaffinger*[1], *S. Stelter*[1], *and F. Uhlig*[1]

[1]Physikalisches Institut IV, Universität Erlangen-Nürnberg, Erwin-Rommel-Str. 1, D-91058 Erlangen

Microchannel-plate (MCP) PMTs will be the most adequate sensors for the PANDA DIRC detectors. They are available as multi-anode devices (e.g., 8×8 pixels) with a sensitive area of 2"×2" and an active area ratio of up to 80%. With ≤10 μm pores they are operable in magnetic fields of 2 Tesla and they provide an excellent time resolution of <50 ps. For a long time the main drawback of MCP-PMTs was severe photo cathode (PC) aging due to ion feedback which led to very short lifetimes. Recently this obstacle has been overcome by coating the MCPs with an atomic layer deposition (ALD) technique. This significantly reduces the flux of ions and the lifetime of MCP-PMTs was increased drastically by a factor of >50 [1].

The lifetime of an MCP-PMT is usually determined by measuring its quantum efficiency (QE) as a function of the integrated anode charge (IAC). In the last years our group has done long-term illuminations of all available lifetime-enhanced MCP-PMT models with the goal of measuring their lifetime under comparable conditions. Every few weeks the gains, dark count rates and QE spectra are measured and plotted as a function of the IAC. In addition a QE scan across the PC surface is performed every few months. The QE results at 400 nm are shown in Fig. 1 for all ALD-coated MCP-PMTs and compared to one tube with a protection film instead of ALD. This illustrates that the 2" XP85112 and the 1" R10754X MCP-PMTs are performing well, while the recently developed 2" Hamamatsu R13266 prototype tubes still need more tuning. The best performing MCP-PMT is currently the PHOTONIS 9001393 with two ALD layers; it reaches 12 C/cm^2 without a deterioration in any performance parameter. At full luminosity this tube would survive 24 years in the PANDA barrel DIRC.

The performance parameters of four new 2" Hamamatsu R13266 MCP-PMTs were further investigated (see also [2]) and in August 2016 they were included in the lifetime setup. On the negative side we observed that the QE across the PC is not yet homogeneous, the gain is varying by almost a factor 10 across the active surface, and the rate capability is only <10^6 photons/cm^2. On the positive side we found a very low dark count rate of well below 100 Hz/cm^2 at most positions and an excellent time resolution of <50 ps even including tails from recoil electrons [3].

A special focus was put on the behavior of the new R13266 inside a magnetic field. Using the high granularity MCP-PMT (128×6 anode pixels) the behavior of the charge cloud was studied. We observed that the charge

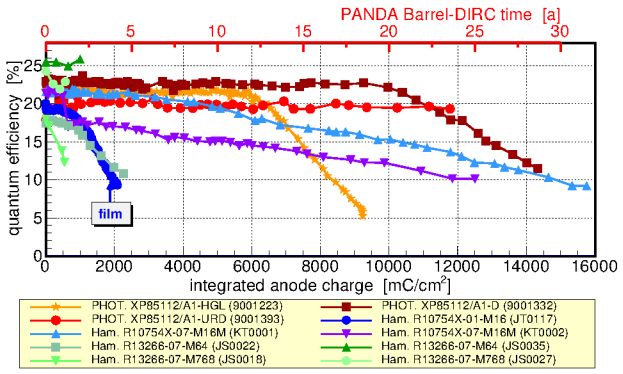

Figure 1: Results of our lifetime measurements for different ALD MCP-PMTs (compared to a tube with film): QE as a function of the IAC at 400 nm (status Jan. 2017).

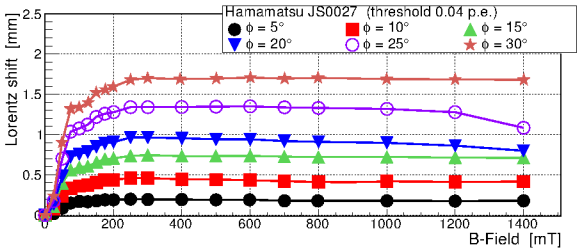

Figure 2: Lorentz shift for different tilt angles ϕ measured inside the 6×128 pixel Hamamatsu R13266 MCP-PMT.

cloud width at the anode plane decreases from 0.7 at no B-field to 0.3 mm at 1.0 Tesla. The cross talk among the anodes turned out to be problematic in this tube and requires further studies. By tilting the PMT axis against the B-field direction at an angle ϕ the Lorentz shift inside the MCP-PMT was determined. With an appropriate setup the cloud centroid shifts along the direction of the high pixelation. By calculating the charge weighted position of the charge cloud the Lorentz shift can be determined. It is specific to every MCP-PMT type and depends upon the inner structure of the tube. In the case of the Hamamatsu R13266-M768 MCP-PMT we observe a maximum shift of 1.7 mm at ϕ = 30° (see Fig. 2). This corresponds to 4 pixels and has to be taken into account in a later analysis of experimental data.

References

[1] A. Lehmann et al., Nucl. Instr. and Meth. A 845 (2017) 570

[2] A. Lehmann et al., https://doi.org/10.15120/GR-2016-1, p. 89

[3] A. Lehmann et al., http://dx.doi.org/10.1016/j.nima.2016.12.063

* Work supported by GSI (contracts EREYRI1416 and ERANTO1419) and BMBF

† Albert.Lehmann@physik.uni-erlangen.de

DOI:10.15120/GR-2017-1

Thickness determination at the cluster-jet target for $\overline{\text{P}}$ANDA*

A.-K. Hergemöller[†1], *D. Bonaventura*[1], *S. Grieser*[1], *B. Hetz*[1], *M. Seifert*[1], *and A. Khoukaz*[1]
[1]Westfälische Wilhelms-Universität, Münster, Germany

The first internal target which will be operated at the $\overline{\text{P}}$ANDA experiment at FAIR is a cluster-jet target. The final $\overline{\text{P}}$ANDA cluster source has been built up [1] in a $\overline{\text{P}}$ANDA-like test setup in combination with the final cluster target beam dump at the University of Münster and has successfully been set into operation as well. Within this kind of target the cluster beam itself is formed by the expansion of pre-cooled gases within a Laval nozzle (further information on Laval nozzles can be found in [2]). To prepare the cluster beam from the surrounding gas-jet two moveable orifices are used, the skimmer and the collimator. Above that, the cluster source includes a nozzle tilting system consisting of a spherical joint with the narrowest point of the Laval nozzle as point of rotation (for more information see [3]). With this feature it is possible to extract highly intense core beams [4], which correspond to regions of higher thicknesses within the cluster beam. For $\overline{\text{P}}$ANDA a target thickness of more than $10^{15}\,\frac{\text{atoms}}{\text{cm}^2}$ in a distance of 2.2 m behind the nozzle is required to achieve the designated luminosity. With the target prototype, operating successfully for years at the University of Münster, it is routinely possible to provide these thicknesses in the required distance. To determine the thickness at the final cluster-jet target for $\overline{\text{P}}$ANDA two different monitor systems are included in the setup. The first one, which will be available later at the $\overline{\text{P}}$ANDA experiment, is an optical monitor system installed in the so called transition vacuum chamber in a distance of 37 cm behind the Laval nozzle. There, the cluster beam is illuminated by a diode laser and is observed by two CCD cameras, which are installed in an angle of 90° to each other. The resulting images of the cluster beam yield information on the position and width of the cluster beam and the intensity distribution corresponds to the relative thickness distribution [5]. To determine the

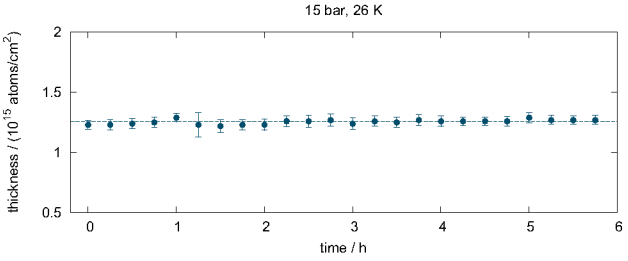

Figure 1: Hydrogen cluster beam stability at stagnation conditions of 15 bar and 26 K at the nozzle inlet.

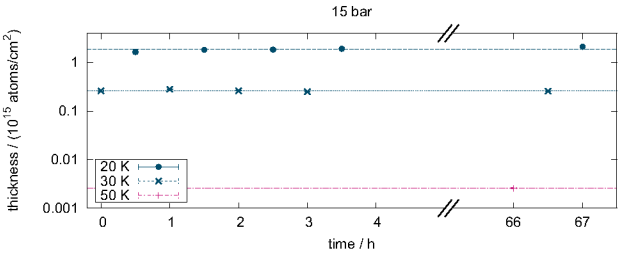

Figure 2: Stability and reproducibility of the target thickness.

absolute target thickness an additional monitor system has been developed and was installed in an interaction chamber in a distance of 1.22 m behind the nozzle. It consists of two rods, which can be moved through the chamber horizontally and vertically. The impinging clusters on the rods affect a pressure increase in the chamber which can be measured for each step of the rod. With this method a profile of the cluster beam is recorded which also yield information on the position and size of the cluster beam. Furthermore, the determination of the maximum pressure increase allows for the measurement of the absolute target thickness [4]. First studies on the thickness and the stability of the cluster beam have been performed successfully. These measurements show that the target thickness is stable over several hours (see Fig. 1) and can be reproduced easily (Fig. 2). Furthermore, the target thickness is easily adjustable over several orders of magnitude by changing the hydrogen stagnation conditions (see Fig. 2). By these measurments the cluster-jet target is proved to meet the expectations and will be installed at the COSY accelerator in Jülich mid 2017 for extensive tests in an experimental environment.

References

[1] A.-K. Hergemöller, "Initial Operation of the Cluster-Jet Target for $\overline{\text{P}}$ANDA", GSI Scientific Report 2015 (2016).

[2] S. Grieser, "Glass Laval Nozzle Prototypes for Cluster-Jet Targets", GSI Scientific Report 2015 (2016).

[3] B. Hetz, Master Thesis, University of Münster, Germany, 2017.

[4] E. Köhler, PhD Thesis, University of Münster, Germany, 2016.

[5] M. Seifert, Bachelor Thesis, University of Münster, Germany, 2016.

* Work supported by HGS-HIRe for FAIR, BMBF and GSI.
† a.hergemoeller@wwu.de

Jet beam analysis with a Mach-Zehnder Interferometer*

S. Grieser†[1], *D. Bonaventura*[1], *A.-K. Hergemöller*[1], *B. Hetz*[1], *L. Lessmann*[1], *C. Westphälinger*[1], *and A. Khoukaz*[1]

[1]Institut für Kernphysik, Westfälische Wilhelms-Universität Münster, Germany

Cluster-jet targets are highly suited for storage ring experiments due to the fact that they provide high and constant beam thicknesses, i.e., up to 10^{15} $\frac{\text{atoms}}{\text{cm}^2}$ in a distance of 2.1 m [1]. Nevertheless, the thickness is adjustable over several orders of magnitude. Therefore, a cluster-jet target is planned to be the first internal target for the $\overline{\text{P}}$ANDA experiment at FAIR. A cluster source generates a continuous flow of cryogenic solid clusters by the expansion of precooled gases within fine Laval nozzles. For the production of clusters and their properties ,i.e., mass distribution, velocity, and formation of high intense core beams, the geometry of the nozzle is crucial. Therefore, an improved nozzle production process based on the initial CERN production was developed and is now established at the University of Münster [2]. To test and ensure the high performance of the Laval nozzles, a Mach-Zehnder interferometer was built up. In this kind of interferometer, one beam is directed through a vacuum chamber, where the Laval nozzle and the cluster-/gas-jet is located, and merges at last with the reference beam. This causes an interference pattern with horizontal interference bands. The expanding jet beam leads to a change in the phase shift (see Fig. 1). The setup is used to visualize the jet beam and also the surrounding gas directly behind the nozzle. Furthermore, the target density and the shape of the beam can be investigated. With this information the geometry of the nozzle, the production process which is influenced by the nozzles geometry, and the stagnation conditions at the nozzle can be optimized and adapted to the experimental requirements.

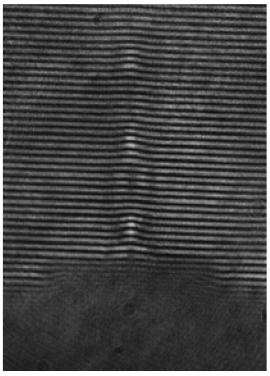

Figure 1: Picture of the interference figure recorded with a CCD camera. At the bottom the shadow of the Laval nozzle exit is visible. Above the nozzle the impact of the gas-jet on the interference bands is observable.

* Work supported by HGS-HIRe for FAIR, BMBF, and GSI

† s.grieser@uni-muenster.de

Above that, an analysis program was created, which calculates the target thickness distribution out of the phase shift from the interference pattern [3]. In a first measurement a nozzle with an inner diameter of 0.5 mm and an outlet diameter of 2 mm was used, which was produced with the new production process at the University of Münster. The applied gas was nitrogen at a temperature of 288 K and a pressure of 20 bar in front of the nozzle. The pressure in the vacuum chamber was varied to study the influence of the pressure in the vacuum chamber on the gas-jet (see Fig. 2). The gas-jet beam expanding into ambient pressure shows the typical shock diamonds which result from the reflection of the jet beam with the surrounding gas in the chamber. Whereas, the expansion into vacuum shows a more divergent and homogeneous shaped beam.

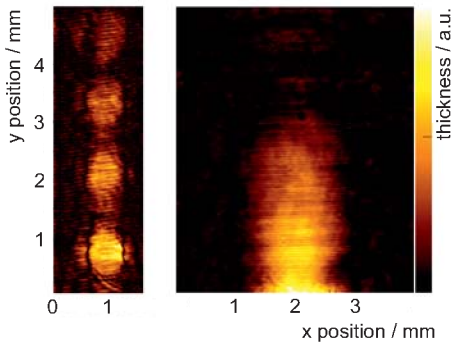

Figure 2: Nitrogen gas-jet, produced at gas pressure of 20 bar and a temperature of 288 K, expands into ambient pressure (left) and vacuum (right).

The Mach-Zehnder interferometer is a powerful analysis system, which offers the possibility to investigate the properties of the jet beam directly behind the nozzle. This leads to a better insight of the formation of clusters and provides more information for the Laval nozzle geometry and their prodction process which is influenced by the nozzles geometry. Additionally, more Laval nozzles with different geometries and their influence on the jet beam will be investigated by this setup in order to provide an optimized set of nozzles for the $\overline{\text{P}}$ANDA experiment.

References

[1] A.-K. Hergemöller, GSI Scientific Report 2016 (2017).

[2] S. Grieser, GSI Scientific Report 2014 (2015).

[3] L. Lessmann, Master thesis, University Münster, Germany, 2016.

DOI:10.15120/GR-2017-1

Gain surface homogeneity of avalanche photodiodes produced in large scale

J. Bailey[1], *A. El Mosleh*[1], *F. Himburg*[1], *D. Scharnberg*[1], *C. Warneke*[1], *P. Wicke*[1], *H. Al-Turany*[1], *I. Retkovac eelja*[2], *and A. Wilms*[1]

[1]GSI, Darmstadt, Germany; [2]Department of Physics, Faculty of Science, University of Zagreb

Introduction

Large area avalanche photodiodes (APDs) are proposed to be used as readout devices of high energy physics electromagnetic calorimeters. According to the high requirements of particle experiments some APD parameters have to be measured to ensure stable conditions of operation. One of them is the homogeneity of the APD surface regarding the internal gain M, whereby the values of M are strongly dependent on applied voltage and temperature.

Gain surface homogeneity of APD

The measured photocurrent of an APD is strongly dependent on the applied bias voltage. In general an amount of 60 to 90 rectangular APDs is cut out of one silicon wafer and several wafers make up one lot. Each wafer or lot will have slightly different characteristics in various parameters, although these differences should not be considerable. Nevertheless it is important to know the profile of eventually occuring current variations over the entire APD surface as well as their possible dependence on lot and wafer number. For this reason the photocurrent homogeneity profile was determined.

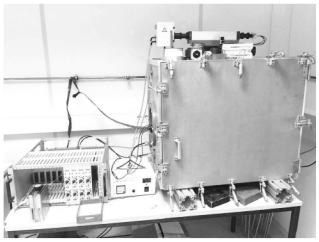

Figure 1: Experimental setup for gain uniformity measurement

Measurement setup

The measurement-stand consists of test chamber, light source and the electronic device transmitting data to a PC via RS232 interface. All components are shown in fig.1. Data acquisition and analysis are done within the ROOT software framework. The needed incident light (420 nm) is provided by a lamp with computer-controlled monochromator mounted on the chamber and guided through a light-fiber bundle into the light-tight chamber. Single APDs are mounted on the x-y-measuring table under one fixed light-fiber. The dark and illumination current are measured for each single diode. The bias voltage values applied are chosen in a regime between 70V to 380V.

Measurements

Measurements were conducted for six wafers originating from different production lots and two wafers of the same lot determined by the specific serial number. We can divide diodes into three district groups - those without direct wafer-neighbours, those with wafer-neighbours on all sides and those originated from the cutting edges of a wafer. The selected APDs represent all three groups. Possible variations of the current over the APD surface could be assigned to the lot/wafer properties or eventually to problems occured during the APD cutting or packaging process.

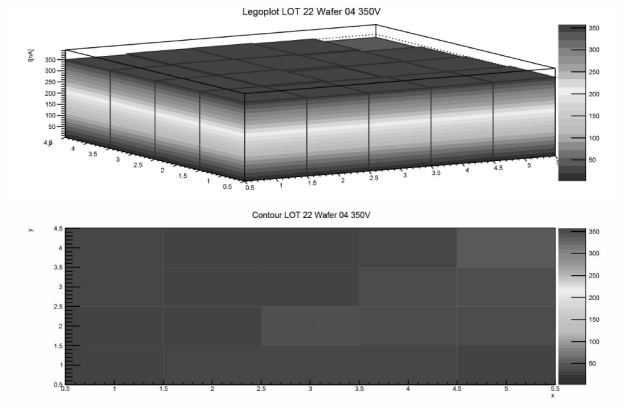

Figure 2: Profile of position-depending APD photocurrent at an applied voltage of 350V (M>30, LOT 22 , Wafer 04, originating from the wafer border).

Based on the prepared measurements the APD photocurrent can be mapped as a function of position, exemplarily shown in figure 2: The x-y plane represents the position on the APD surface and the z axis represents the measured photocurrent in nA. The variation of current over the surface was found to be on the level of a few percent of the mean value.

Preliminary results

The homogeneity of the APD photocurrent over the device surface was determined. The tested APDs originated from different lots and for each lot subsamples of a few wafers were picked out. The determined photocurrent values were found to be nearly constant, independent of surface position or of the applied bias voltage value. APDs from the cutting edges of a wafer seem to apparently show a slightly higher deviation in the measured photocurrent. Further measurements have to be prepared for confirmation.

DOI:10.15120/GR-2017-1

Large area avalanche photo diode irradiation at Giessen*

M. Moritz†[1], *K.-Th. Brinkmann*[1], *H.-G. Zaunick*[1], *and for the* $\overline{P}ANDA$ *collaboration*[1]
[1]II. Physikalisches Institut, Justus-Liebig-Universität Giessen, Germany

The electromagnetic target calorimeter (EMC) [1] of the future $\overline{P}ANDA$ detector has the challenging aim to detect high energy photons with excellent energy resolution from 15 GeV down to a few tens of MeV. To reach this goal, improved $PbW0_4$ scintillator crystals, cooled down to $-25°C$ and read out with two precisely matched large area avalanche photo sensors (APD) each, have been choosen. In order to ensure the stable and reliable high precision operation over the whole envisaged lifetime, the radiation hardness of each photo sensor has to be verified. Furthermore, the parameters of a matched pair, especially the high voltages for each APD, have to develop in a very similar way under the radiation dose which will be accumulated during the whole lifetime of the experiment. To fulfill these requirements, the APDs have to undergo a sophisticated screening and matching procedure. One main step of this procedure is therefore the irradiation with a high intensity ^{60}Co γ-source at the irradiation facility in Giessen.

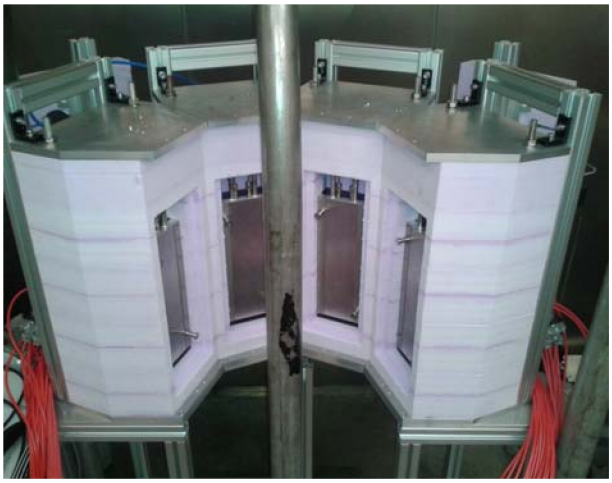

Figure 1: APD irradiation setup at the ^{60}Co irradiation facility at Justus Liebig University Giessen.

The customized setup, as partly shown in figure 1, allows a well controlled irradiation procedure. Four so-called grids, holding twenty APDs each, can be irradiated simultaneously under individual bias for every single APD. Due to the temperature-dependent bias voltage for a certain gain, each grid sits in a separate temperature-isolated box. These boxes are equipped with a liquid-based cooling system in order to facilitate a temperature-stable environment at $20°C$ and are located at a distance of $25.5\ cm$ around the source. The γ-source, which can be mechanically moved into the vertical metal tube in front of the setup, provides nowadays a dose rate of $37\ Gy/h$ at the distance of the setup. The integrated dose of one hour corresponds to the maximum dose which one APD should accumulate within 10 years of $\overline{P}ANDA$ operation.

On the background of the future mass production for the whole calorimeter, which requires processing of nearly 30.000 APDs, the following procedure was iteratively elaborated. After a first screening procedure via the Photo Sensor Laboratory (PSL) [2], the APDs are delivered for irradiation to Giessen. Before each irradiation, the electronic contact of all APDs is verified by measuring the generated current under illumination at 0 Volts bias. After a few minutes for temperature equalization, the dark currents are measured. Furthermore, the dark currents during and after irradiation with $37\ Gy$ under bias were recorded. The present irradiation procedure allows to irradiate up to 400 APDs within a normal working day. In the end, all delivered APDs and the corresponding data are sent back to the PSL for a second screening procedure. The second procedure includes an annealing process for recovering radiation damages. During the second half of 2016, all APDs for the first EMC barrel slice went trough the whole procedure of the irradiation in Giessen. The integrated total screening procedure throughput with an increasing slope can be seen in figure 2.

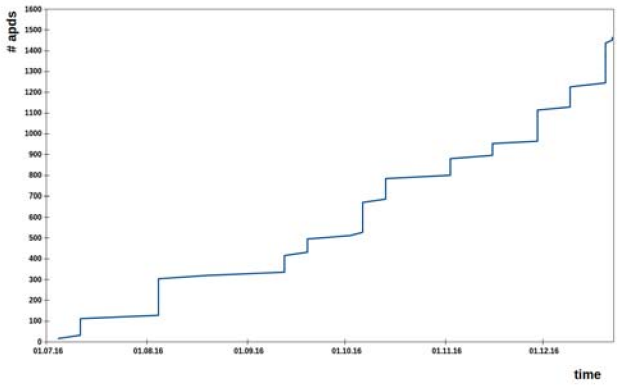

Figure 2: Amount of APDs which passed the screening process since the beginning of the first slice assembly project in 2016.

* This Work is supported by BMBF, GSI and HIC4FAIR.
† markus.moritz@exp2.physik.uni-giessen.de

DOI:10.15120/GR-2017-1

References

[1] PANDA COLLABORATION, Technical Design Report for the $\overline{P}ANDA$ Electromagnetic Calorimteter. arXiv:0810.1216 [physics.ins-det], 2008.

[2] https://www.gsi.de/work/forschung/detector_laboratory/psl.htm

Investigation of aging effects in GEM detectors*

B. Ketzer[†1], *M. Ball*[1], *C. Dreisbach*[2], *and R. Schmitz*[1]

[1]Universität Bonn, Helmholtz-Institut für Strahlen- und Kernphysik, 53115 Bonn, Germany; [2]Technische Universität München, Physik Department, 85748 Garching, Germany

An element-specific analysis of depositions on GEM foils exposed to a high-intensity particle beam has been performed. We identify traces of Si and S in the affected regions. Several materials such as glue and conformal coating used in the construction of the detectors are tested for their composition in order to identify the source of the deposition. A setup to systematically study the influence of outgassing from materials on GEM detectors is presented.

Introduction

Detectors based on charge amplification in micropattern structures such as the Gas Electron Multiplier (GEM) [1] exhibit a much higher rate capability than conventional multi-wire proportional chambers (MWPC). Particle rates beyond $1 \cdot 10^6\,\mathrm{mm^{-2}s^{-1}}$ have been reached without noticeable gain reduction [2, 3]. Spatial resolutions of the order of $70\,\mu\mathrm{m}$ are routinely achieved with a projective strip readout in high-intensity environments [4]. In addition, GEM detectors can be built with an extremely small material budget of the order of 2–3 per mill of a radiation length [3]. It is for these reasons that three stations of large planar GEM detectors are foreseen as forward trackers in the PANDA barrel spectrometer [5]. An application as particle beam monitors is also conceivable. When operating such detectors for a long time in a high-intensity particle beam, even tiny contaminations of the gas from outgassing materials used for detector construction or in the gas lines can severely compromise the performance. The foreign molecules will be ionized in the avalanche process and the resulting ions will follow the electric field lines to an electrode, where they are neutralized and deposited. In order to avoid this, it is vital to carefully investigate the outgassing properties of all materials used in the construction of a GEM detector and thus qualify them for their suitability.

Depositions on GEM foils

A set of planar triple-GEM detectors with pixel readout [6] have been subjected to high-intensity muon and hadron beams at CERN. After accumulating a total charge of more than $10\,\mathrm{mC/mm^2}$, significant inefficiencies became visible in the region exposed to the beam, caused by severely reduced signal pulse heights. Opening the detector, a change of color correlated with the inefficient region clearly indicated that depositions of unwanted contaminations on the GEM foils are responsible for the effect.

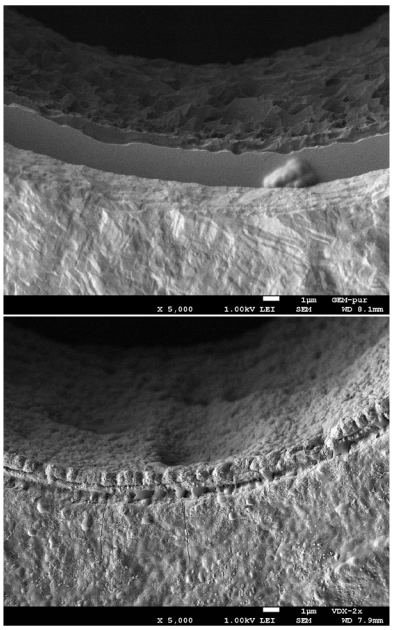

Figure 1: Scanning electron microscope picture of GEM holes, (top) of a new foil, (bottom) of a foil after accumulation of more than $10\,\mathrm{mC/mm^2}$.

In order to further study the depositions, samples of a damaged foil were investigated using a scanning electron microscope (SEM, type JEOL - JSM 7500F) and compared to a new one. Fig. 1 shows (top) a GEM hole in an unused foil and (bottom) a hole in the foil exposed to the beam. While the Cu surface and the Polyimide insulator are clearly visible on the top figure, the damaged hole at the bottom figure clearly depositions of material around and inside the hole, rendering the edge of the metal surface indistinguishable from the insulator.

Energy-dispersive X-ray spectroscopy

The elemental composition of the deposits was analyzed by detecting the X-rays which are emitted following the bombardment of the foil by electrons in the SEM (Energy dispersive X-ray spectroscopy, EDX). Figure 2 shows the EDX spectra (top) for the new foil, and (bottom) for the damaged foil. There are clear traces of Silicon (Si) and Sulfur (S) on the damaged foil, corresponding to an atomic fraction of 1.5% and 5.3%, respectively.

* Work supported by GSI cooperation with University of Bonn, contract no. BNKETZ1416

† Bernhard.Ketzer@uni-bonn.de

DOI:10.15120/GR-2017-1

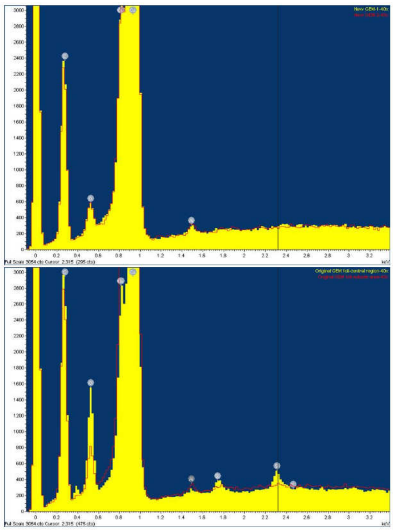

Figure 2: EDX spectra of (top) a new GEM foil and (bottom) a damaged GEM foil. Clear traces of Si and S are found on the damaged one.

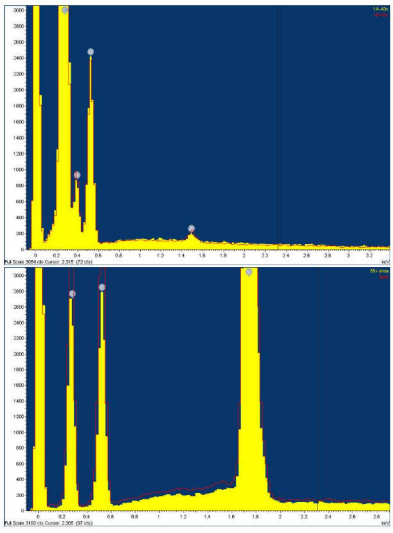

Figure 3: EDX spectra of (top) Araldit AY103-1/HY991 (glue/hardener) and (bottom) Dow Corning 1-2577 conformal coating.

In the following, we analyzed several materials used in the construction of the detectors in the same device, including glue (Araldit AY103-1/HY991), and a conformal coating (Dow Corning 1-2577) used to seal the detector from the outside. The corresponding EDX spectra are shown in Fig. 3. The results indicate that the Silicon originates from the conformal coating. The origin of Sulfur is not yet fully understood, but could be due to sulfuric acid (H_2SO_4) used for cleaning during the production process of the readout circuit.

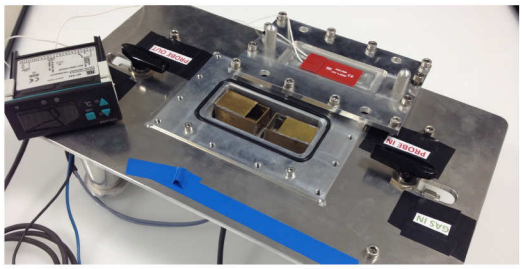

Figure 4: Temperature-stabilized sample box for the controlled introduction of impurities into a gaseous detector through the input gas line.

Setup for aging measurements

A dedicated setup was built to systematically analyze the outgassing properties of materials and their influence on the performance of GEM detectors. Figure 4 shows a photograph of a sample box developed for material tests. The device is mounted in the input gas line to the detector, such that any outgassing molecules are transported to the detector. The cavern is temperature-stabilized up to 70° to accelerate outgassing. It can also be used to add ppm-amounts of other pollutants like H_2O in a controlled way to the detector gas [7]. The device will be used in a measurement campaign dedicated to study the aging effects induced by different materials.

Summary

The results of the aging investigations revealed a clear deposition of Si and S on GEM foils after their exposure to a high particle flux. The contaminations stem from materials used for the construction of the detector, noticeably from a conformal coating which apparently crept into the detector. Also agents used in the production process of special components like readout circuits may be critical. Further investigations will be performed to clarify the origin of Sulfur. These results are relevant for all applications where GEM detectors are exposed to high particle fluxes, like in the PANDA experiment.

References

[1] F. Sauli, Nucl. Instr. Meth. A 386 (1997) 531.

[2] J. Benlloch et al., Nucl. Instrum. Meth. A419 (1998) 410.

[3] COMPASS, P. Abbon et al., Nucl. Instr. Meth. A 779 (2015) 69, 1410.1797.

[4] B. Ketzer et al., Nucl. Instr. Meth. A 535 (2004) 314.

[5] PANDA Collaboration, M. Lutz et al., (2009), 0903.3905.

[6] B. Ketzer et al., Nuclear Science Symposium Conference Record, 2007. NSS '07. IEEE Vol. 1, pp. 242–244, Piscataway, NJ, 2007, IEEE.

[7] S. Urban, Development of QA procedures for large-area GEMs, Master's thesis, Rheinische Friedrich-Wilhelms-Universität Bonn, 2016.

DOI:10.15120/GR-2017-1

Performance study of the $\overline{\text{P}}$ANDA GEM-tracker in the physics simulation*

N. Divani Veis[†1,2,3], *R. Karabowicz*[1], *T. Saito*[1,2], *B.Voss*[1], *and the $\overline{\text{P}}$ANDA collaboration*[1]

[1]GSI, Darmstadt, Germany; [2]HIM, Mainz, Germany; [3]University of Birjand, Iran

To provide measurement of charged particles trajectories with high resolution over the solid angles, one of the inner tracking system is the $\overline{\text{P}}$ANDA GEM-tracker to cover the forward solid angles below 22 degrees. A gas electron multiplier (GEM) is a type of the gaseous ionization detector which will be used as a first forward tracking detector behind the central tracker in the $\overline{\text{P}}$ANDA experiment. This work is investigation of the influence of the GEM-tracker to improve the track finding efficiency and track momentum resolution in the $\overline{\text{P}}$ANDA setup.

Investigation of the track finding efficiency and track momentum resolution

In this investigation is used the realistic pattern recognition for track reconstruction procedure in order to understand the behaviour of the $\overline{\text{P}}$ANDA GEM-tracker in different momenta and angles of emitted particles in the forward directions of interest (below 22 degrees). The particles tracking approach is aimed to reconstruct the particles trajectories in all the inner trackers system (STT, MVD, and GEM tracking detectors) in the target spectrometer of the $\overline{\text{P}}$ANDA setup simultaneously [1]. Briefly, this algorithm loops over all the hits created in different detectors and matches them first to already existing tracks and subsequently to unused hits. This algorithm focuses on the primary trajectories, that is the ones emerging from or around the interaction point. The comparison between the true and the reconstructed momenta allows to determine the track momentum resolution as well [2].

To investigate the track finding efficiency and track momentum resolution, fifty thousand events of the single charged particles (pions) are propagated for two selected values of the momentum 0.5, and 5 GeV/c using the current implemented GEM geometry with three stations [3]. The particles are emitted in the range of the polar angles (θ) between 2 to 45 degrees and the azimuthal angles (ϕ) between 0 to 360 degrees. For each values of the theta and momentum of pions the simulation is done separately in two cases: the full $\overline{\text{P}}$ANDA setup with GEM-tracker (with contributions of the three inner trackers STT, MVD, and GEM together) and without GEM-tracker (with contributions of the two inner trackers STT and MVD only) for track finding procedure. To check and compare the influence of the GEM-tracker to improve the quality of the track finding efficiency, Figure 1 and Figure 2 show the polar angular distribution of the track finding efficiency and track momentum resolution respectively. The contributions and performance of the GEM-tracker are visible at the plots for the 0.5, and 5 GeV/c at the covering polar angles below 22 degrees. Of course, the contributions of the other trackers (STT and MVD) are large to reconstruct tracks for the large angles which are not related to the region of the GEM-tracker.

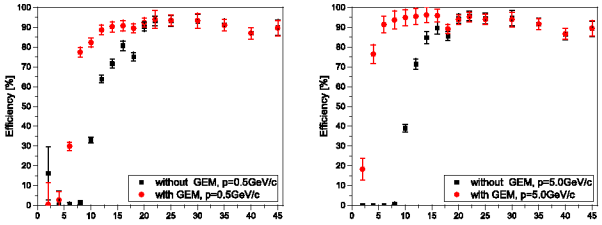

Figure 1: The polar angular distribution of the track finding efficiency for two selected values of pions momenta 0.5 GeV/c (left), and 5 GeV/c (right) in two cases: $\overline{\text{P}}$ANDA setup with (circular points) and without (squared points) the GEM-tracker. The single pions are propagated in the range of the θ polar angles between 2 to 45 degrees and the ϕ azimuthal angles between 0 to 360 degrees. The rounded points indicate the good track finding efficiencies in the forward directions of interest.

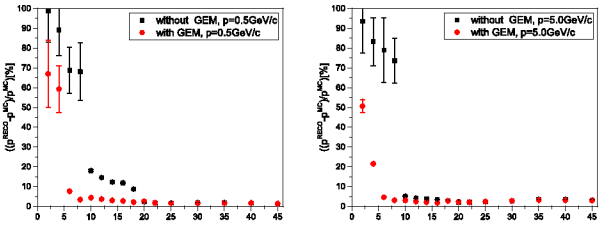

Figure 2: The track momentum resolution versus θ polar angles for two selected values of pions momenta 0.5 GeV/c (left), and 5 GeV/c (right) in two mentioned cases.

References

[1] B. Voss, GSI Scientific Report 2008(2009) 242.

[2] R. Karabowicz, GSI Scientific Report 2010(2011) 117.

[3] N. Divani Veis et al., GSI Scientific Report 2015(2016) 92.

* Work supported by HI Mainz (GEM Technologies (4316))

† n.divani@gsi.de

DOI:10.15120/GR-2017-1

Estimation of the fractional radiation length for the current designed geometry of the $\overline{\text{P}}$ANDA Planar-GEM tracker*

N. Divani Veis† [1,2,3], *R. Karabowicz*[1], *T. Saito*[1,2], *B.Voss*[1], *and the $\overline{\text{P}}$ANDA collaboration*[1]

[1]GSI, Darmstadt, Germany; [2]HIM, Mainz, Germany; [3]University of Birjand, Iran

In the $\overline{\text{P}}$ANDA experiment, charged particles proceeding to the forward directions with the polar angles approximately between 2 to 22 degrees will be measured by a set of large-area planar gaseous micro-pattern detectors equipped with GEM foils as amplification stages. This study presents the estimation of the fractional radiation length for the implemented $\overline{\text{P}}$ANDA GEM-Tracker in Monte-Carlo simulation. This includes the current conceptual technical design of the realistic GEM geometry.

Detector description for the $\overline{\text{P}}$ANDA GEM-tracker

The $\overline{\text{P}}$ANDA GEM-tracker stations are in form of circular planes (disk shape). The geometry of the $\overline{\text{P}}$ANDA GEM detectors in the simulation was transported from the designed geometry implemented in the CAD software [1, 2]. The tracking system contains three stations of planar GEM including main layers and holding support structures. Each station realizes a complex series of multi-layers with aluminium windows, cathodes, GEM foils, sensitive pad planes, Ar/CO_2 gas containers, cooling support and electronic devices. Each of GEM foils and pad planes consists of three thin layers with the copper-kapton-copper configuration.

The double-sided read-out pad planes are located in the centre of each station providing strip information about crossing particles in four projections: radial and circular in front side, horizontal and vertical in back side. The total radius and the Z position (along the beam line in the Cartesian coordinate originating from the target center) of each station respectively are 45 and 119.4 cm for the first station, 56 and 155.4 cm for the second station and 74 and 188.5 cm for the last one. The Riddle shell with its rigid and light-weight supporting structures which holds all the GEM-tracker stations have also been implemented with carbon fiber [3, 4]. The entire GEM system with three stations and the supporting structure is shown in Figure 1.

Estimation of the Fractional Radiation Length for the $\overline{\text{P}}$ANDA GEM-tracker

To study about the effect of the material of the GEM stations for charged particles passing through the detectors, one of the beneficial concepts is to estimate the radiation length. It adds up in all the traversed volumes, depending on the specific radiation length ($X0$) and the density of the materials defined for the volumes corresponding to the traversed path length therein [5].

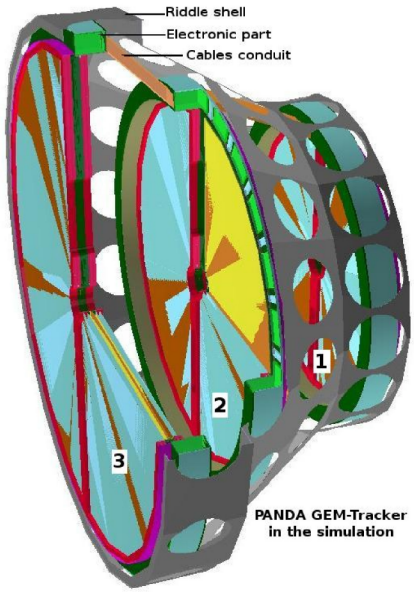

Figure 1: The entire layout of the $\overline{\text{P}}$ANDA GEM-tracker with the current realistic geometry implemented in the PandaRoot. It includes three stations with the main layers in aluminium, kapton and copper, the drift layers with Ar/CO_2 mixed gas, the support structures in carbon and glass fiber, the electronic parts in copper, the cables conduit in copper, and also the Riddle shell in carbon fiber to hold all parts of the detector together.

The introduction of the detailed geometry provides precise quantification of the amount of material introduced the detector in different regions. As the GEM is located in front of the detectors in upstream in the Target Spectrometer as well as of the all the detectors of the Forward Spectrometer, it will influence the track reconstructions with these detectors in forward directions. Thus, we studied the effect of the GEM components by means of the radiation length.

For estimating of the GEM materials budget and extracting of the GEM materials map, the virtual particles "Geantinos" [6] were propagated through the detector using Geant4 simulation engine. These fictitious particles undergo no physical interactions but flag boundary crossings along their straight trajectories and counting the number of the radiation lengths crossed by them within the GEM.

* Work supported by HI Mainz (GEM Technologies (4316))

† n.divani@gsi.de

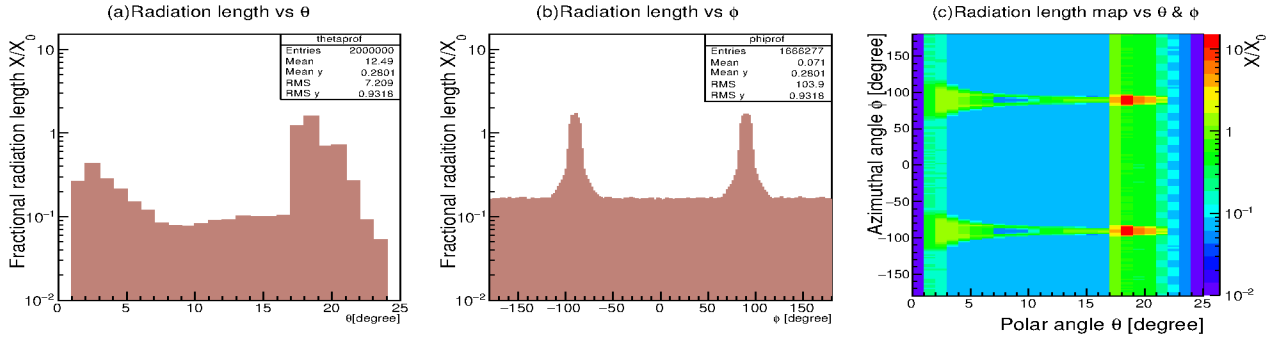

Figure 2: The results of the radiation length for the entire $\overline{\text{P}}$ANDA GEM-tracker geometry. This figure consists of: (a) the fractional radiation length versus polar angle,θ, (b) the fractional radiation length versus azimuthal angle, ϕ, and, (c) the map of the radiation length, θ versus ϕ. They are evaluated by propagating two million Geantinos in ranges from 0 to 25 degrees for θ and from 0 to 360 degrees for the ϕ. In addition, the radiation length map shows the changes which are belonged to the main layers, holding support structures and electronics sections placed in this regions. The changes displayed in red belong to the cables conduit and the changes in blue inside the green belong to the shape of the holding structures and their vertical holes in both side in the GEM geometry).

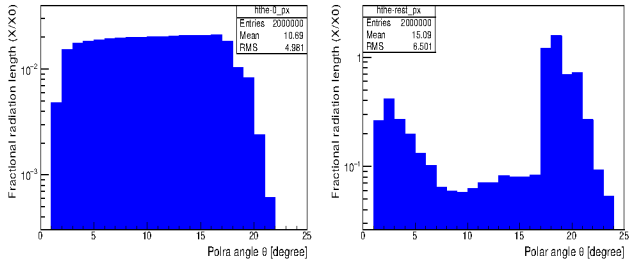

Figure 3: The results of the radiation length separately for the main layers and holding support structures and electronic parts of the $\overline{\text{P}}$ANDA GEM-tracker geometry. This figure consists of: (left) the fractional radiation length versus polar angle,θ for main layers, and, (right) the fractional radiation length versus polar angle, θ for the holding support structures and electronic parts. They are evaluated by propagating two million Geantinos in ranges from 0 to 25 degrees for θ and from 0 to 360 degrees for the ϕ.

In order to have more exact information, profiles of the polar angle (θ) and the azimuthal angle (ϕ) are provided for the contribution of the different GEM components. Two millions of particles were generated at the target position with the polar angle (θ), and the azimuthal angle (ϕ), respectively distributed flatly in ranges from 0 to 25 degrees, and from 0 to 360 degrees. Figure 2 and 3 demonstrate the results of the fractional radiation length for the presented $\overline{\text{P}}$ANDA GEM-tracker geometry.

Figure 2 shows the distributions of the radiation length defined as $X/X0$ as functions of θ and ϕ respectively in the left and middle panels for the entire GEM geometry with three stations. A two-dimensional distribution of $X/X0$ in the θ-ϕ plane (as a map of the radiation length) is also shown in the right panel in the figure. In most of the regions, the radiation length $X/X0$ is below 10^{-1}. However, larger $X/X0$ values exceeding one are distributed around $\theta = 18°$ and $\phi = \pm 90°$. In order to specify the contributions to those large $X/X0$ values, distributions of $X/X0$ as functions of θ and ϕ are separately studied for the main layers and support structures (the holding structures, electronics and cables conduit), as shown in Figure 3. The study of radiation length for the GEM detector and their associated structures has shown that the $X/X0$ values are below 10^{-2} for the main layers of the GEM stations.

References

[1] B. Voss et al., GSI Scientific Report 2008(2009) 242.

[2] B. Voss et al., GSI Scientific Report 2009(2010) 338.

[3] R. Karabowicz et al., GSI Scientific Report 2009(2010) 12.

[4] N. Divani Veis et al., GSI Scientific Report 2015(2016) 92.

[5] S. Bianco et al., "The CAD model of the $\overline{\text{P}}$ANDA Micro-Vertex-Detector in physics simulation", Nuclear Instrument and Methods in physics Research A, 654(2011)630-633.

[6] Geant4 Toolkit, Webpage: http:geant4.cern.chsupport/proc_mod_catalog/particles .

DOI:10.15120/GR-2017-1

Investigation of the $\Lambda\,\overline{\Lambda}$ invariant mass reconstruction with the $\overline{\mathrm{P}}$ANDA Planar-GEM tracker*

N. Divani Veis[†1,2,3], *R. Karabowicz*[1], *T. Saito*[1,2], *B.Voss*[1], *and the $\overline{\mathrm{P}}$ANDA collaboration*[1]

[1]GSI, Darmstadt, Germany; [2]HIM, Mainz, Germany; [3]University of Birjand, Iran

One important part of the physics program of the $\overline{\mathrm{P}}$ANDA experiment is to study about hyperons and their structures. Hyperons decay weakly and they have a long life time and mean decay length. This causes to have also the hyperons decay in the outer part of the central tracker of the $\overline{\mathrm{P}}$ANDA setup. In this work, simulation have been fulfilled for the $\overline{\mathrm{P}}$ANDA GEM-tracker with $\overline{\Lambda}\Lambda$ decay channel in order to perform acceptance studies. $\overline{\mathrm{P}}$ANDA GEM-tracker is a set of large-area planar gaseous micro-pattern detectors equipped with GEM foils which will measure charged particles proceeding to the forward directions with the covering polar angles approximately between 2° to 22°.

$\Lambda\,\overline{\Lambda}$ Mass resolution

$\Lambda\,\overline{\Lambda}$ channel has been chosen because Λ is the lightest hyperon which is easiest to produce and all final state particles are charged. The full $\overline{\mathrm{P}}$ANDA setup based on the PandaRoot framework has been used in two cases with the GEM-tracker (with contributions of the three inner trackers STT, MVD, and GEM together) and without GEM-tracker (with contributions of the two inner trackers STT and MVD only) in order to study and compare the behaviour and the performance of the current designed GEM-tracker [1, 2] in this physics decay channel. The mentioned reaction was simulated at beam momenta of 2GeV/c of the boosted antiprotons by generating fifty thousand events to study real state of interaction as the forward peaking. The simulations have done with the realistic pattern recognition for the track finding procedure [3]. Figure 1 shows the invariant mass reconstruction and the polar angular distribution for the simulated Λ and $\overline{\Lambda}$ with (red) and without (black) GEM-tracker in the $\overline{\mathrm{P}}$ANDA setup. In right panel (up and down) of this Figure is demonstrated the Λ and $\overline{\Lambda}$ mass reconstruction for all possible combinations of the related particles in this decay channel. The mean values and the mass resolutions of two cases are shown in Table 1. In left panel of this Figure is also implied a big improvement using GEM-tracker to show the reconstructed Λ and $\overline{\Lambda}$ in forward directions of interest (below 22 degrees). The influence of the GEM-tracker in order to improve the mass reconstruction in this channel are also visible in the Armenteros plots in Figure 2. In these plots, the transverse momentum of the decay products in the Λ rest frame is plotted as a function the asymmetry α, where $\alpha = \frac{p_{L+}-p_{L-}}{p_{L+}+p_{L-}}$ and $p_{L+(-)}$ is the longitudinal momentum of the positive (negative) particles produced in this decay. In this Figure the Armenteros plots obtained for both setups without (left) and with (right) GEM-tracker.

Table 1: The mass resolutions and reconstruction efficiency for the Λ and $\overline{\Lambda}$ invariant mass reconstruction with and without GET-Tracker in the $\overline{\mathrm{P}}$ANDA setup.

for all combination of particles	without GEM Λ	with GEM Λ	without GEM Λ (antiΛ)	with GEM Λ(antiΛ)
Mean Value [GeV/c^2]	$1.118\pm3.164\times10^{-4}$	$1.116\pm2.075\times10^{-4}$	$1.120\pm4.966\times10^{-4}$	$1.115\pm1.538\times10^{-4}$
Mass Resolution [GeV/c^2]	$0.020\pm4.828\times10^{-4}$	$0.018\pm2.255\times10^{-4}$	$0.026\pm6.934\times10^{-4}$	$0.017\pm1.733\times10^{-4}$
Reconstruction Efficiency[%]	15.57	27.35	19.34	62.37

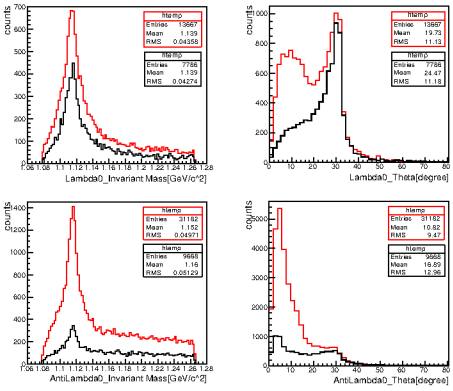

Figure 1: The invariant mass reconstruction and polar angular momentum of the simulated Λ and $\overline{\Lambda}$ with (red) and without (black) the GEM-tracker in the $\overline{\mathrm{P}}$ANDA setup.

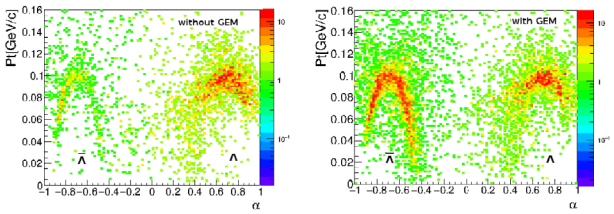

Figure 2: The Armenteros plots obtained with (right) and without (left) the GEM-tracker in the $\overline{\mathrm{P}}$ANDA setup at the beam momentum of 2GeV/c.

References

[1] B. Voss et al., GSI Scientific Report 2009(2010) 338.

[2] N. Divani Veis et al., GSI Scientific Report 2015(2016) 92.

[3] R. Karabowicz et al., GSI Scientific Report 2009(2010) 117.

* Work supported by HI Mainz (GEM Technologies (4316))

† n.divani@gsi.de

A precision lineshape measurement of the $X(3872)$ with PANDA/FAIR

F. Nerling[1,2], *K. Götzen*[1], *R. Kliemt*[3], *K. Peters*[1,2], *and the PANDA Collaboration*[1]
[1]Goethe Univ. Frankfurt, Germany; [2]GSI, Darmstadt, Germany; [3]HIM, Mainz, Germany

The first of the new charmonium-like states discovered since 2003, the $X(3872)$ [1], is still one of the most puzzling ones concerning the properties. Since the mass is indistinguishable close to the sum $m(D^0) + m(\bar{D}^{*0})$, it is unclear whether it lays above or beneath the DD^* threshold. Furthermore, the natural width is very small and basically unknown up to a rather rough upper limit of Γ_X<1.2 MeV/c^2 [2]. Due to these extra-ordinary properties, this state is frequently suggested to be an exotic hadron, possibly featuring a different and more complex internal structure than a simple conventional mesonic $q\bar{q}$ state. In particular, several theoretical models (e.g. [3]) relate not only the mass m_X and the Breit-Wigner-like width Γ_X to the internal structure, but explicitly also the lineshape of the resonance.

This offers another experimental handle to identify the nature of the $X(3872)$, however, a precise measurement is beyond the scope of currently running experiments. Due to typical detector resolutions (∼8 MeV), the precision needed to resolve this very narrow structure in subsequent decays is not reached, unless the $X(3872)$ with $J^{PC} = 1^{++}$ is created in a formation reaction $A+B \to X$ with excellent beam energy precision as it will be delivered by HESR/FAIR, allowing for a resonance energy scan. This is not possible for resonances with $J^{PC} \neq 1^{--}$ in an e^+e^- experiment — in $\bar{p}p$ annihilation reactions, however, all $q\bar{q}$-like spin-parity states can directly be produced in formation, see also [4].

We have studied the expected sensitivity of energy scans of narrow resonances performed with the HESR in combination with the PANDA detector at FAIR [5] under various assumptions of signal cross sections, input widths and luminosities. Apart from the quantification of the prospected sensitivity for the width and lineshape measurement of the example of the $X(3872)$, this exemplary analysis serves as a proof of principle for high precision spectroscopy using the energy scan method with the PANDA experiment in general.

The projected sensitivity for a Breit-Wigner like width as obtained for a PANDA/FAIR phase-1 measurement (i.e. HESRr mode, reduced luminosity) based on 20 energy scan points (two days of data taking per point) within a 1.4 MeV window around the nominal mass is summarised in Fig. 1. The scanned cross-section after de-convolution of the known beam profile together with the Breit-Wigner fit is exemplarily shown for an assumed input width of $\Gamma_0 = 130$ keV (Fig. 1, top) together with the obtained relative uncertainties that will be achieved for a range of assumed input widths Γ_0 beneath 1 MeV. A twenty percent relative uncertainty is achieved for an input width of

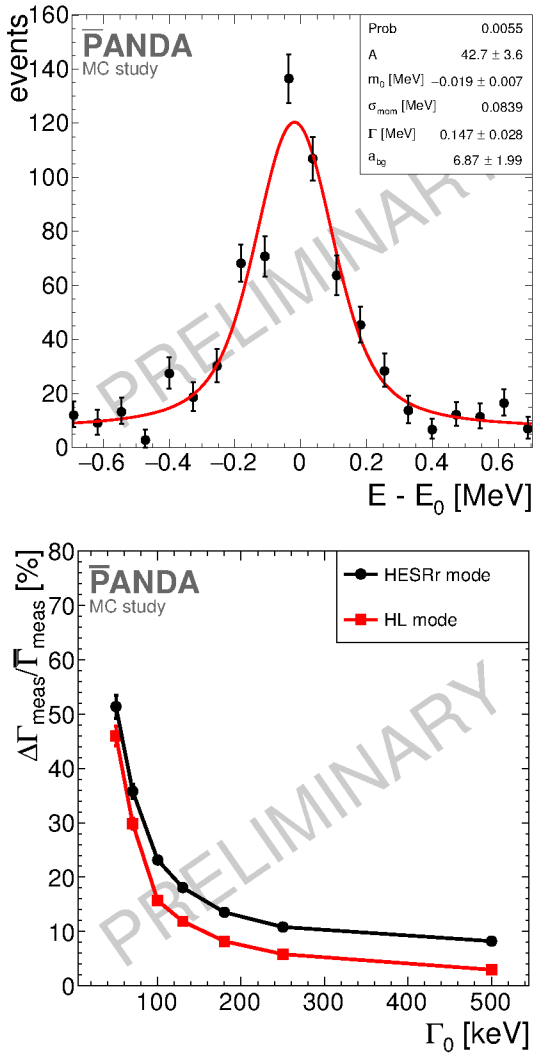

Figure 1: Full MC simulation study of a resonance energy scan using the example of the very narrow $X(3872)$.

Γ_0=100 keV, and the obtained resolution is better for the high luminosity (HL) mode (Fig. 1, low). These results have been released by the PANDA Collaboration and are planned to be published in a journal article soon.

References

[1] Belle Collab., S.-K. Choi *et al.*, PRL 91 (2003) 262001.

[2] K.A. Olive *et al.* (Particle Data Group), Chin. Phys. C 38, 090001 (2014), and 2015 update.

[3] C. Hanhart *et al.*, PRD 76 (2007) 034007.

[4] F. Nerling *et al.*, GSI Scientific Report 2015-1, (2015) 117.

[5] PANDA Collab., W. Erni *et al.*, arXiv:0903.3905 [hep-ex].

DOI:10.15120/GR-2017-1

Chiral anomaly in the baryonic sector of the eLSM *

L. Olbrich[1], *M. Zétényi*[2,3], *F. Giacosa*[1,4], *and D. H. Rischke*[1]

[1]Institute for Theoretical Physics, Goethe University, Frankfurt am Main, Germany; [2]Wigner Research Center for Physics, Budapest, Hungary; [3]ExtreMe Matter Institute EMMI, GSI Helmholtzzentrum für Schwerionenforschung, Darmstadt, Germany; [4]Institute of Physics, Jan Kochanowski University, Kielce, Poland

We consider the so-called extended linear sigma model (eLSM). For the case of $N_f = 3$, it contains (pseudo)scalar and (axial-)vector mesonic degrees of freedom [1] as well as glueballs [2, 3]. In order to reproduce known properties of the strong interaction, it features explicit and spontaneous breaking of chiral symmetry, as well as the $U(1)_A$ anomaly. Only recently, this model has been further extended to include also three-flavor baryonic fields describing four spin-$\frac{1}{2}$ baryon multiplets [4]. These additional fields allow to introduce a further chiral anomaly term in the baryonic sector, which will be investigated in this work.

Since every effective model should (to some extent) show the pattern of flavor symmetry, we first consider a simple model which features *only* the symmetry under $U(N_f)_V$ transformations. Although a model like this is very limited due to the lack of chiral symmetry, it appears to be useful to set a framework for further studies. We construct a Lagrangian which is flavor symmetric, as well as invariant under parity and charge-conjugation transformations. This allows to study the decays of negative-parity baryonic resonances into ground-state positive-parity baryonic states and one pseudoscalar meson. In fact, we investigate two distinct models, where in each one a different negative-parity baryon octet is described: first the octet $\{N(1535),\ \Lambda(1670),\ \Sigma(1620),\ \Xi(?)\}$, and second the heavier states $\{N(1650), \Lambda(1800), \Sigma(1750), \Xi(?)\}$.
As a result of the first model, we found that the flavor symmetry works well to describe most of the decay widths, but with important mismatches: flavor symmetry clearly underestimates (values are too small by around one order of magnitude) the decay widths of the octet resonances $\{N(1535),\ \Lambda(1670),\ \Sigma(1620),\ \Xi(?)\}$ into ground-state baryon states and one η meson.
On the contrary, in the second model where the excited states describe the heavier resonances $\{N(1650), \Lambda(1800), \Sigma(1750), \Xi(?)\}$, the decays into the η meson are in agreement with the experimental data.
The inability to describe certain decays into η properly shows that an additional component is needed when the η meson is considered.

A possible approach to solve this problem is the inclusion of the $U(1)_A$ anomaly. To investigate this idea in detail, we introduce a chiral anomaly term in the baryonic sector of eLSM. To this end, we use the baryonic fields and their properties as introduced in Ref. [4] to extend the Lagrangian by a term that is invariant under parity and charge conjugation, as well as $SU(3)_L \times SU(3)_R$ transformations. It contains two parameters of dimension [energy^{-2}], each one of them describing the coupling of either two equal- or different-parity baryon fields to the object

$$\det \Phi - \det \Phi^\dagger \,, \tag{1}$$

where the 3×3 matrix Φ describes the nonet of (pseudo)scalar mesons. The determinants in Eq. (1) ensure the explicit breaking of the symmetry under $U(1)_A$ transformations. Using the matrix form of Φ (as given in Ref. [1]) we obtain that the expression of Eq. (1) is proportional to the fields η_N and η_S (plus further terms with more than one meson field). Consequently, the anomaly term, which is the coupling of two baryon fields to this object, enhances the interactions with η and η' (being the physical fields that arise from admixtures of η_N and η_S).

As a further test, we incorporated this anomaly term (with only two baryonic fields and one parameter) into the flavor-only model described at the beginning. After fitting the parameter to the decay width of $N(1535) \to N\eta$, the improved model now reproduces also the decay width of $\Lambda(1670) \to N\eta$. This shows that the increase caused by the anomaly term is in agreement with the data from experiment. Furthermore, the model predicts an enhanced coupling to η' through the inclusion of the anomaly.

References

[1] D. Parganlija, P. Kovacs, G. Wolf, F. Giacosa and D. H. Rischke, Phys. Rev. D **87** (2013) 1, 014011 [arXiv:1208.0585 [hep-ph]].

[2] W. I. Eshraim, S. Janowski, F. Giacosa and D. H. Rischke, Phys. Rev. D **87** (2013) no.5, 054036 doi:10.1103/PhysRevD.87.054036 [arXiv:1208.6474 [hep-ph]].

[3] W. I. Eshraim, S. Janowski, A. Peters, K. Neuschwander and F. Giacosa, Acta Phys. Polon. Supp. **5** (2012) 1101 doi:10.5506/APhysPolBSupp.5.1101 [arXiv:1209.3976 [hep-ph]].

[4] L. Olbrich, M. Zétényi, F. Giacosa and D. H. Rischke, Phys. Rev. D **93** (2016) 3, 034021 [arXiv:1511.05035 [hep-ph]].

* Work supported by HGS-HIRe / HQM, the Hungarian OTKA Fund No. K109462, ExtreMe Matter Institute EMMI, and NCN OPUS project 2015/17/B/ST2/01625.

Investigation of a charmed scalar tetraquark candidate*

J. Berlin†[1] *and M. Wagner*[1]

[1]Goethe-Universität Frankfurt am Main, Institut für Theoretische Physik, Max-von-Laue-Straße 1, D-60438 Frankfurt am Main, Germany

The discovery of the positive parity charmed mesons $D^*_{s0}(2317)$ [1] and $D_{s1}(2460)$ [2, 3] at the BaBar, Belle and CLEO has attracted much interest as a structure beyond conventional quark-antiquark states might apply. For our first lattice study we investigate a $D^*_{s0}(2317)$ candidate regarding a possible four-quark structure. This state is of lower mass than predicted by many quark models and the $D^*_{s0}(2317) - D^*_0(2400)$ mass difference is too small to account for the s-u/d quark mass difference.

Utilizing the variational method we aim to study the heavy tetraquark candidate $D^*_{s0}(2317)$, close to the neighboring $D_s\pi$ and $D\bar{K}$ thresholds. We compute two-point correlation functions of two-quark and four-quark interpolating operators of different structure including quark-antiquark type, mesonic molecule type, diquark-antidiquark type and two-meson type, i.e.

$$\begin{aligned}
\mathcal{O}^{q\bar{q}} &= \frac{1}{\sqrt{V_s}} \sum_{\mathbf{x}} \Big(\bar{c}(\mathbf{x}) s(\mathbf{x})\Big), \\
\mathcal{O}^{D\bar{K},\,\text{point}} &= \frac{1}{\sqrt{V_s}} \sum_{\mathbf{x}} \Big(\bar{c}(\mathbf{x})\gamma_5 u(\mathbf{x})\Big)\Big(\bar{u}(\mathbf{x})\gamma_5 s(\mathbf{x})\Big), \\
\mathcal{O}^{D_s\pi,\,\text{point}} &= \frac{1}{\sqrt{V_s}} \sum_{\mathbf{x}} \Big(\bar{c}(\mathbf{x})\gamma_5 s(\mathbf{x})\Big)\Big(\bar{u}(\mathbf{x})\gamma_5 u(\mathbf{x})\Big), \\
\mathcal{O}^{Q\bar{Q}} &= \frac{1}{\sqrt{V_s}} \sum_{\mathbf{x}} \epsilon_{abc}\Big(\bar{u}_b(\mathbf{x})(C\gamma_5)\bar{s}^T_c(\mathbf{x})\Big) \\
&\qquad \epsilon_{ade}\Big(c^T_d(\mathbf{x})(C\gamma_5)u_e(\mathbf{x})\Big), \\
\mathcal{O}^{D\bar{K},\,\text{2part}} &= \frac{1}{V_s} \sum_{\mathbf{x},\mathbf{y}} \Big(\bar{c}(\mathbf{x})\gamma_5 u(\mathbf{x})\Big)\Big(\bar{u}(\mathbf{y})\gamma_5 s(\mathbf{y})\Big), \\
\mathcal{O}^{D_s\pi,\,\text{2part}} &= \frac{1}{V_s} \sum_{\mathbf{x},\mathbf{x}} \Big(\bar{c}(\mathbf{x})\gamma_5 s(\mathbf{x})\Big)\Big(\bar{u}(\mathbf{y})\gamma_5 u(\mathbf{y})\Big).
\end{aligned}$$

This is done by employing the most efficient lattice techniques or combination of techniques [4] to provide the best possible signal at comparable computational costs.

The resulting correlation matrix C yields of a tower of states with the quantum numbers of interest ($J^P = 0^+$)

$$C_{jk}(t) = \langle \mathcal{O}_j \mathcal{O}^\dagger_k \rangle = \sum_{n=0}^{\infty} \langle 0|\mathcal{O}_j(t)|n\rangle \, \langle n|\mathcal{O}^\dagger_k(0)|0\rangle \, e^{-E_n t}.$$

These states can be extracted from the eigenvalues after solving a generalized eigenvalue problem

$$C(t)\, v_n(t,t_0) \;=\; \lambda_n(t,t_0)\, C(t_0)\, v_n(t,t_0),$$

$$E_n = \lim_{t\gg a} E^{\text{eff}}_n(t,t_0) = \lim_{t\gg a} \frac{1}{a} \log \frac{\lambda_n(t,t_0)}{\lambda_n(t+a,t_0)}.$$

The so-called *effective masses* that are obtained from various operator bases regarding our correlation matrix are shown in Figure 1.

We observe a third low-lying state with an indication of a structure beyond the conventional quark-antiquark interpretation. Although the state is dominated by a $q\bar{q}$ signal (violet), it is also observed without employing two-quark structures (yellow). In the presence of both dominating contributions is a four-quark component is still sizeable.

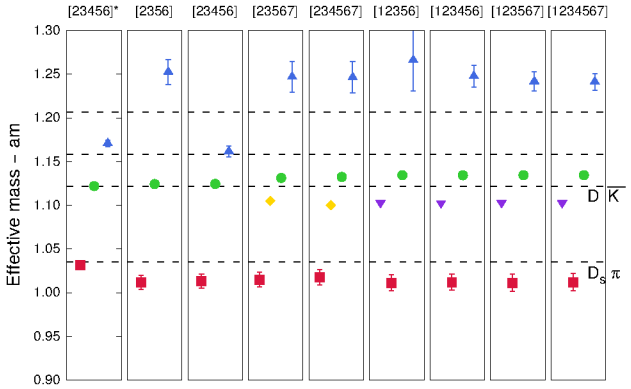

Figure 1: Observed states for $m_\pi \approx 300$ MeV from various interpolator bases, referring to $1 \equiv q\bar{q}$, $2;3 \equiv D\bar{K}$, point; $D_s\pi$, point, $5;6 \equiv D\bar{K}$, 2part; $D_s\pi$, 2part, $4;7 \equiv$ light; heavy $Q\bar{Q}$ interpolating field operators.

References

[1] B. Aubert *et al.* [BaBar Collaboration], Phys. Rev. Lett. **90**, 242001 (2003) doi:10.1103/PhysRevLett.90.242001 [hep-ex/0304021].

[2] K. Abe *et al.* [Belle Collaboration], Phys. Rev. Lett. **92**, 012002 (2004) doi:10.1103/PhysRevLett.92.012002 [hep-ex/0307052].

[3] D. Besson *et al.* [CLEO Collaboration], Phys. Rev. D **68**, 032002 (2003) Erratum: [Phys. Rev. D **75**, 119908 (2007)] doi:10.1103/PhysRevD.68.032002, 10.1103/PhysRevD.75.119908 [hep-ex/0305100].

[4] A. Abdel-Rehim, C. Alexandrou, J. Berlin, M. Dalla Brida, J. Finkenrath and M. Wagner, arXiv:1701.07228 [hep-lat].

* Work support by — the Emmy Noether Programme of the DFG (German Research Foundation), grant WA 3000/1-1 — the Helmholtz International Center for FAIR within the framework of the LOEWE program launched by the State of Hesse

† berlin@th.physik.uni-frankfurt.de

DOI:10.15120/GR-2017-1